JPhys Energy

TOPICAL REVIEW • OPEN ACCESS

Accelerating the development of new solar absorbers by photoemission characterization coupled with density functional theory

Journal of Physics: Energy

TOPICAL REVIEW

Accelerating the development of new solar absorbers by photoemission characterization coupled with density functional theory

Tim D Veal[1], David O Scanlon[2,3,4], Robert Kostecki[5] and Elisabetta Arca[5,*]

[1] Stephenson Institute for Renewable Energy and Department of Physics, University of Liverpool, Liverpool L69 7ZF, United Kingdom
[2] Department of Chemistry, University College London, 20 Gordon Street, London WC1H 0AJ, United Kingdom
[3] Thomas Young Centre, University College London, Gower Street, London WC1E 6BT, United Kingdom
[4] Diamond Light Source Ltd, Diamond House, Harwell Science and Innovation Campus, Didcot, Oxfordshire OX11 0DE, United Kingdom
[5] Energy Storage and Distributed Resources Division, Lawrence Berkeley National Laboratory, Berkeley, CA 94720, United States of America
[*] Author to whom any correspondence should be addressed.

E-mail: earca@tcd.ie **and** earca@lbl.gov

Keywords: solar absorbers, x-ray photoelectron spectroscopy, density functional theory, band alignment, solar cells

OPEN ACCESS

RECEIVED
26 October 2020

REVISED
11 January 2021

ACCEPTED FOR PUBLICATION
3 March 2021

PUBLISHED
25 March 2021

Abstract

The expectation to progress towards Terawatts production by solar technologies requires continuous development of new materials to improve efficiency and lower the cost of devices beyond what is currently available at industrial level. At the same time, the turnaround time to make the investment worthwhile is progressively shrinking. Whereas traditional absorbers have developed in a timeframe spanning decades, there is an expectation that emerging materials will be converted into industrially relevant reality in a much shorter timeframe. Thus, it becomes necessary to develop new approaches and techniques that could accelerate decision-making steps on whether further research on a material is worth pursuing or not. In this review, we will provide an overview of the photoemission characterization methods and theoretical approaches that have been developed in the past decades to accelerate the transfer of emerging solar absorbers into efficient devices.

1. Introduction

A better understanding of the implications of fossil-fuel produced energy on climate changes and pollution, coupled with a steady decline of the cost of solar-produced electricity, has created an expectation for PV to progress towards multi-Terawatts capacity, with goals set for 10 TW of PV-produced energy by 2030 and 30–70 TW by 2050 [1]. PV market leaders such as silicon (∼95% of the market in 2018), cadmium telluride or copper indium gallium selenide, however, will be unable to fulfil this demand. Some of the limitations of Si-based solar cells include the energy intensive process required for the Si purification [2, 3] and a precious metal, silver, to produce the electrical contacts [1]. Although CdTe and copper indium gallium selenide (CIGS) solar cells are undoubtedly the competitors at a market level to Si [4–6], the toxicity and scarcity of some of their constituent elements have kept the search for more suitable solar absorbers very much alive in the past decades [7]. The discovery of hybrid perovskite solar cells and widespread of related research have boosted the field even more, due to the extraordinary gain in performance that these absorbers have shown. It is natural that the research community has made tremendous efforts into understanding the fundamental mechanism responsible for their outstanding performance and possibly, design materials that could have the same performance without the instability limitation that hybrid perovskite display [8–15]. With the advent of high-throughput calculations and data-mining algorithms capable of predicting hundreds of new compounds in a relative short space of time [10, 14, 16–22], pressure has increased to provide experimental validation of the quality and merit of these predicted materials. Growth of new materials and their

characterization can be substantially accelerated by high-throughput methods [23–25], and recently these methods have been extended to full device fabrication [26–33] and interphase characterization [34]. However, the conversion of new materials into highly performing device is often still slow and inefficient, requiring several years if not decades in most cases.

Among solar absorbers, certainly the hybrid organic–inorganic perovskite represent an exception in terms of rapid performance gains, virtually fulfilling the Holy Grail-quest for defect-tolerant semiconductors [8, 9, 13, 35, 36]. However, the issue of long-term stability and problems with scaling to large area-devices has so far hampered a reliable and substantial market penetration [37, 38]. Thus, it has become essential to develop methodologies that can accelerate turnover of new materials into market-relevant highly performing devices, whether this means improving their efficiency or their long-term stability.

For emerging solar absorbers, efficiency above 10% is often challenging. As rule of thumb, such efficiency can be obtained for materials having carrier lifetime of at least 1 ns [39]. It has to be emphasized that this is a minimum condition, *necessary but not sufficient* to ensure the realization of high-performing devices. In some cases, control over the bulk properties represents the shortcoming, like for example the high carrier concentration of $ZnSnN_2$ [40–43]. In other cases, realization of an efficient cell was not successful even if the bulk material was promising. Examples of this kind include Zn_3P_2 [44, 45] and Cu_2O [46], for which good minority carrier lifetimes and large bulk carrier diffusivity have been reported, however device efficiencies are below the breakthrough 10% threshold [46, 47]. Lack of good junction partners, property degradation upon device fabrication and inherent or induced instability upon operation might all be key limitations to achieve highly performing and stable solar cells. So how do we overcome these bottlenecks?

In this review, we will examine some of the required bulk properties that new semiconductors should exhibit in order to be plausible candidate as solar absorber materials (section 2). Once the basic bulk properties have been established, the role of the interface becomes the key-challenge to achieve good and stable devices (section 3). To this end, photoemission spectroscopies have been pivotal to determine the 'goodness' and 'badness' of a given interface. This means being able to assess the chemical stability and compatibility of two materials when brought into contact, and how the alignment of their bands would favor or disfavor the extraction of the photogenerated carries. The use of the high-vacuum soft x-ray and ultra violet photoelectron spectroscopies (XPS and UPS) or hard x-ray photoelectron spectroscopy (HAXPES) in some cases combined with near ambient pressure (NAP-XPS) will be discussed in the context of solar absorbers. The merit of these techniques and the different regime of validity when applied to PV will be reviewed in section 3. With the advent of modern computing, the experimental characterization of materials and interfaces largely benefited from a complementary theoretical and experimental approach. In section 4 of this review, we will provide an overview of the application of density functional theory (DFT) calculations for the development of emerging solar absorbers, with particular emphasis on the design of new materials and understanding of the interfacial properties in the device. Finally, traditional application of XPS methods has expanded in several fields with the development of *in-operando* characterization, i.e. characterization of the constituent materials when the device is under operational conditions with the possibility of correlating materials' properties to device performance parameters. The field of solar absorbers is no exception to this trend and its application to measure the quasi-Fermi level splitting in a passivated solar absorber [48, 49] will be reviewed in section 5.

2. Comparison of bulk vs interface phenomena—limiting factors on the widespread of new solar absorber—a brief overview

The tremendous success of the hybrid-perovskite has contributed to the definition and has progressively become more entangled with the concept of 'defect tolerance' [8, 10, 50–52]. This expression indicates the capability of a material to retain high power-conversion efficiency despite the presence of defect and grain boundaries, or, in other terms, the ability of a material to tolerate such defects without forming deep levels in the band gap that could act as recombination centers for photogenerated minority carriers [10, 50] (see figure 1).

In a defect-tolerant material, intrinsic or extrinsic defects (impurities) are still present but they give rise to exclusively shallow levels [10, 50, 56] (figure 1). This manifests itself in the transition level diagrams such as those shown in figure 1, where the transition levels, marked as the change in the slope of the formation energy of a given defect, lie very close to the band edges, forming the so called 'shallow level'. Such type of defects have an exponentially lower contribution to non-radiative recombination rates [57]. In contrast, in defect 'intolerant' materials, such transition levels are deep in the band gap and so are called 'deep levels' and thus they can act as recombination centers. The macroscopic result of this behavior is that materials such as MAPI display long minority carrier lifetimes and power-conversion efficiency approaching the Shockley–Queisser (SQ) limit [50].

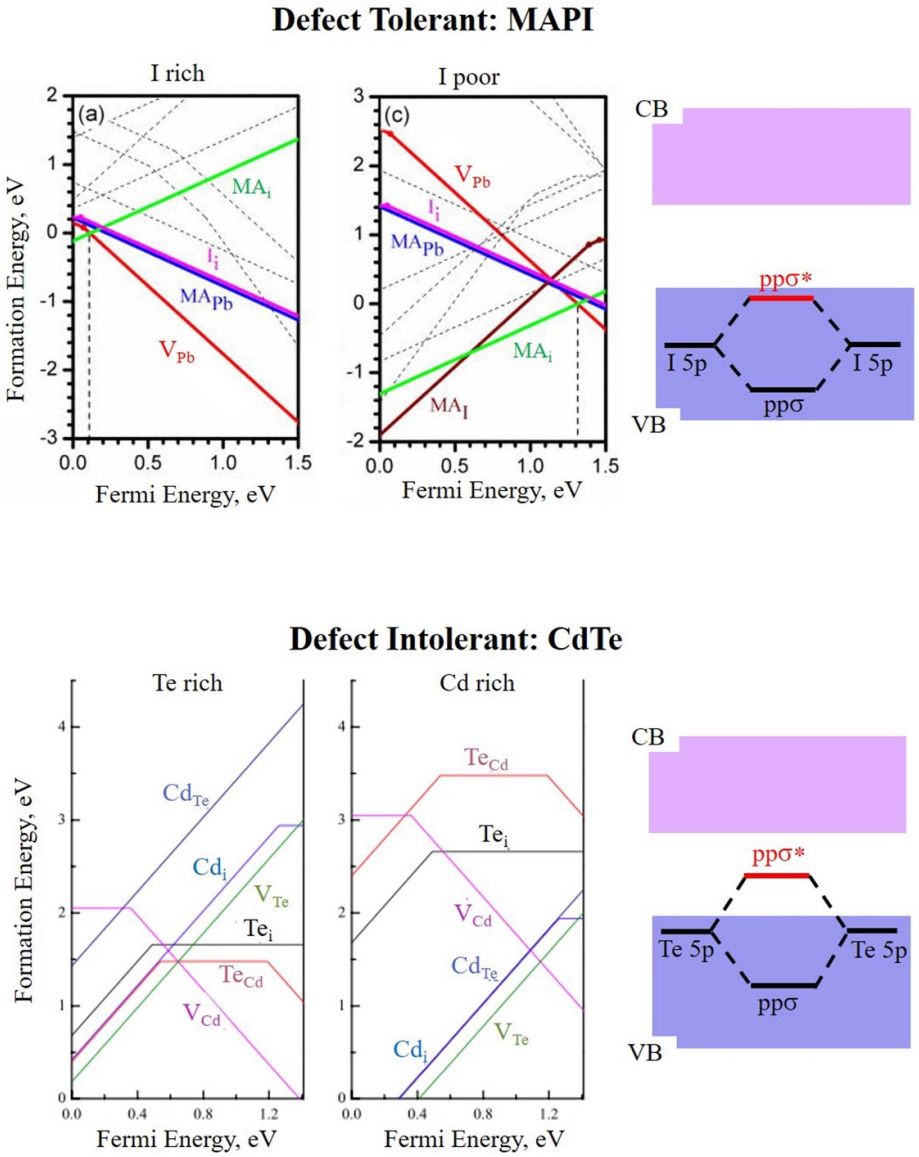

Figure 1. Defect tolerant vs intolerant material. The transition phase diagram shows that the transition points lay within or very close to the band edges (shallow levels) for the methylammonium lead iodide (MAPI) case (Reprinted and adapted from [53], with the permission of AIP Publishing), whereas these levels are deep in the gap for the case of CdTe (Reprinted and adapted with permission from [54]. Copyright (2013) by the American Physical Society). Such deep levels can act as recombination centers, limiting the minority carrier lifetime, contrary to MAPI, whose defect chemistry favors long minority carrier lifetimes. The molecular description with bonding and antibonding characters is reported as well (Reproduced from [55] with permission of The Royal Society of Chemistry).

The magnitude of the band gap, rather than the relative abundance and non-toxicity of the constituent elements, has been in many cases the determining factor for assessing the potential of a new material for PV. This is because until recently, the material selection was based largely on the SQ limit, and thus the predictor for a highly-efficient PV absorber was mainly based on the magnitude of the band gap and on a high absorption coefficient. This has led to a number of materials, which, despite the scientific merit of the investigations, would hardly satisfy the requirements to be commercially relevant solar absorbers after more than a decade of research. Example of this kind includes: Cu_2O-based solar cells, for which solar cells were reported since the mid-70s [58], and after several decades its record efficiency is lagging behind the 10% threshold (9.54% for a Si-junction [59], 8.1% for all-oxide junctions [60]); $ZnSnN_2$, firstly grown in 2012 [61] and with the best efficiency to date at 1.54% [62]; CZTS, whose champion efficiency has raised to 12.6% in 2013 [63]; SnS which has been studied for the past two decades [64, 65] and the best record efficiency achieved so far is only 4.36% [66]; Zn_3P_2 studied since 1979, whose record efficiency is still only of about 6% [47]; Cu_xS was anticipated to be a promising earth-abundant solar absorbers in the early 1980s, with a reported record efficiency above 10% [67]. However the mobility of the Cu vacancy lead to sever instability and difficulties in determining the exact crystal structure both experimentally and theoretically [68–70].

Compensating doping by Sn has been recently proposed as a method to induced stability in the material, reviving the interest in this earth-abundant non-toxic semiconductor [70]. A complete list of emerging solar absorbers and related devices characteristics can be found in [71].

Recent works highlighted how factors other than the band gap—such as minority carrier diffusion length, absorption coefficient as a function of wavelength, internal/external quantum efficiencies—are crucial materials properties which might limit the efficiency of a material well-below the value predicted by the SQ-limit [56, 72, 73].

Among these, the minority carrier lifetime is probably one of the most easily accessible from an experimental standpoint. Together with the minority carrier mobility, the lifetime determines the diffusion length of minority carriers according to equation (1) [74].

$$L_{\mathrm{diff}} = \sqrt{D\tau_{\mathrm{bulk}}} \tag{1}$$

$$D = \sqrt{\frac{k_{\mathrm{B}}T}{q}}\mu \tag{2}$$

where L_{diff} is the bulk diffusion length, D is the diffusivity, τ_{bulk} is the bulk lifetime, k_{B} is the Boltzmann constant, q is the electronic charge, and μ is the mobility. Thus, it is extremely important to be able to determine experimentally both the minority carrier lifetime and their mobility *reliably*.

With respect to minority carrier lifetime, a number of techniques are available to determine it, yet care needs to be taken when assessing the results, particularly for new materials. For a mature technology like silicon, the experimental methodologies and the assumptions involved in the data analysis are well established and thus the value extracted are usually quite accurate. The same does not hold true for new materials. Severe variations in the value of the lifetime extracted for a given material have been reported due to the difficulties in interpreting the data [50]. Often not all the physical parameters required to correctly interpret the experimental data are known [39, 75] and for materials where detrapping is the mechanism dominating the time-resolved photoluminescence measurements, overestimation of minority carrier lifetimes and a lack of correlation between the latter and the device performance, particularly the V_{OC}, have been reported [76, 77]. Despite the potential risk of overestimating minority carrier lifetimes, assessing this physical property is of fundamental importance in determining whether or not a prospective material warrants further investigation. It is worth mentioning that in terms of achieving long carrier lifetime, both defect concentration (defect physics of the material) and the capture cross section of a given defect play a role. The defect physics of the materials will be discussed in section 4. As for the capture cross section, the high dielectric constant of hybrid-perovskite has been proven to be beneficial in terms of reducing the capture cross section of defects and thus increasing the minority carrier lifetimes [10, 12]. In addition to considering bulk recombination mechanisms, recombination at grain boundaries and at the surfaces (or interfaces) has to be considered. Passivation of the interface to reduce recombination through defects and improve extraction of the photogenerated carrier will be discussed in details in section 3.

The second parameter affecting minority carrier diffusion is the minority carrier mobility. Experimental determination of this quantity is not trivial and, particularly for emerging absorbers, is sometimes derived from majority carrier mobility and the ratio of the majority and minority carrier effective masses [78]. Despite difficulties in the experimental determination of this quantity, its magnitude is extremely relevant for the development of future solar absorbers. The role of mobility can also explain why many of the high-performing absorbers are p-type and far less are the n-type. In p-type absorbers, electrons are the minority carriers, which take advantages of usually a highly disperse conduction band. In comparison, n-type absorbers have holes as minority carriers. The valence bands are often less disperse than conduction bands and thus hole mobility is often lower than electron mobility, negatively affecting the charged-carrier extraction [78]. It is worth mentioning that the low effective masses for both hole and electrons is a contributing factor to the success of hybrid-perovskites, which display long minority carrier lifetime for both holes and electrons [79].

A final bulk-property worth mentioning is the doping level. Device fabrication requires careful control of this property which affects key parameters such as the electrical resistivity of the materials (and thus the serial resistance), the depletion width and the Fermi level splitting (and thus the V_{OC}) [80]. Although it is not the only factor, the position of the band edges with respect to vacuum have a very important effect both in terms of the doping levels achievable in a semiconductor and the spontaneous formation of charge compensating defects [81–83]. The latter not only determine the pinning of the Fermi level in terms of doping levels, but often compensating defects lie deep in the band gap and thus act as recombination centers.

In conclusion, in order for a material to warrant further consideration as a prospective solar absorber, it should display high minority carrier diffusion length or at least lifetime, strong solar absorption matched to

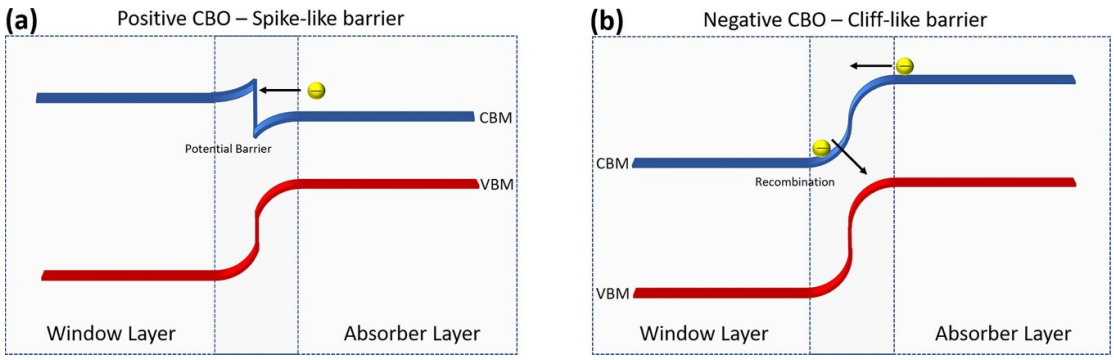

Figure 2. (a) A positive CBO, leading to a spike-like barrier at the interface and (b) a negative CBO giving a cliff-like barrier at the interface. Reproduced from [99]. CC BY 4.0.

the solar spectrum, abundance and possibly non-toxicity of its constituent elements and a doping level in the range suitable to solar application.

3. Interface characterization

Once the basic materials properties are achieved, the next step is the device fabrication. Interfaces play a major role in any photovoltaic device, and poorly designed interfaces could lead to a completely non-working device no matter how good the bulk properties of the absorbers are. Moreover, correct device architecture that optimizes charge separation and minimizes recombination at the interfaces, is another major bottleneck for emerging solar absorbers.

Many solar absorbers were derived by cation permutation to replace expensive or rare elements with more abundant and cheaper analogues. Examples of this kind includes CIGS (copper indium gallium diselenide) derived from cation permutation from CdTe (II-VI) to CIGS (I-III-VI_2). From further permutation of the group III elements indium and gallium, which were replaced by II-IV elements Zn and Sn, leads to copper zinc tin sulfide CZTS (I_2-II-IV-VI_2). Later on the series continued with the discovery (or borrowing from mineralogy) of $CuSbS_2$ and Cu_3BiS_3 derived as analogous to CIGS after replacement of In and Ga with Sb or Bi [84–87]. Similarly the II-IV-V_2 materials arose by cation transmutation of III-V semiconductors, with $ZnSnN_2$ derived by cation permutation to, for example InN, where the group III element (In) is replaced by Zn and Sn, and which has been reported as a potential solar absorber by several groups [40–42, 61, 62, 88–91]. In the case of perovskite inspired materials, the number of perovskite or double perovskite inspired by the original MAPI is very large and the reader is referred to some of the seminal papers and reviews in the field, and references within [8, 92–95].

In the first attempts to make a device using a new solar absorber, particularly for those absorbers derived by cation permutation, researcher almost naturally adopted the device structure of the parental material. Examples of this kind include perovskite-inspired materials, for which a p–i–n structure with hole and electron transport layers are used [96] or junctions with CdS being used for CIGS-derived $CuSbS_2$ [87] and SnS. Interestingly, the contact layer widely used with chalcogenides-based absorbers, CdS, has, however, been proven to be a poor choice in terms of band alignment in a number of cases including SnS, Cu_3BiS_3 and $CuSbS_2$ [84, 85, 97, 98]. Indeed there is no guarantee that the device architecture that works for the parental absorber would work equally well for the emerging solar absorber under investigation. As device fabrication process is a time-consuming and expensive task, it becomes of paramount importance to adopt the experimental and theoretical approaches that can identify immediately non-working device architectures, to avoid pitfalls and waste of resources.

At a device level, the choice of partner materials that maximize the achievable open circuit voltage and thus the cell efficiency is crucial. Band alignments between the absorber and its junction partner (often called window layer) can be detrimental if the conduction band offset (CBO) is too large in either direction. Positive and negative CBOs are depicted in figure 2 for the case of a p-type absorber where the minority carriers are electrons. For the case of a positive CBO, there will be a spike-like barrier which will impede electron transport across the junction. For a negative CBO, there will be a cliff-like barrier, which leads to a small energy separation between the conduction and valence bands at the interface, giving a pathway for recombination and reducing the obtainable V_{OC}. It is thus crucial to find a good candidate absorber that avoids either type of unfavorable alignment.

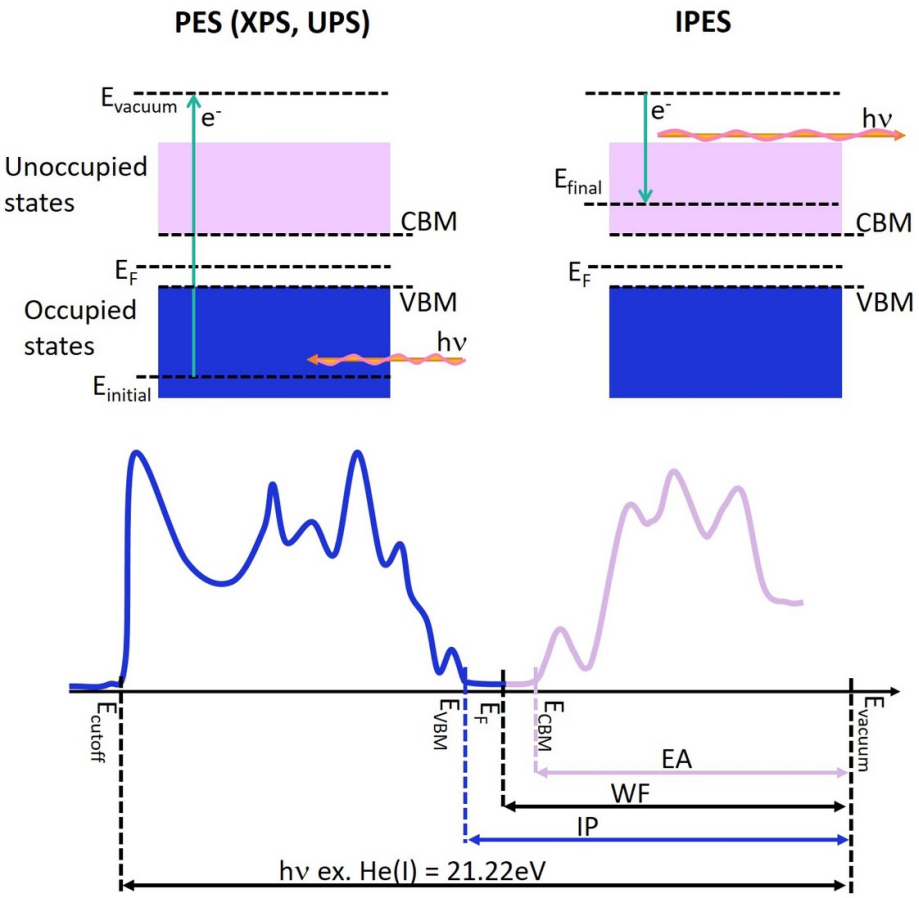

Figure 3. Comparison between the physical principle of photoemission spectroscopy (XPS, UPS), and inverse photoemission spectroscopy (IPES). The diagram further explain how the measured quantities (EA, WF, IP) correlates with the band structure of the material.

In order to determine the partner material for a particular absorber in a device, it is sensible to determine the absorber's band alignment with respect to the vacuum level and thereby its alignment with the bands of the potential partners' materials (natural band alignment). The ionization potential (IP) (VBM to vacuum level separation) can be determined experimentally by a combination of XPS and UPS [84, 85, 100] or theoretically by DFT calculations [90, 101–104].

There are at least five distinctly different experimental approaches to determining the band alignments between two materials. The first is based on determining the natural band alignments of each material with respect the vacuum level by measuring the IP. The second begins as the first method and then proceeds with the application of the so-called electron affinity (EA) rule to align the bands of two materials. The third uses the Kraut method to directly determine the valence band offset (VBO or ΔE_V) between two materials using measurements of a real interface between them, along with measurements of 'bulk'-like layers of the two materials. The fourth method involves the use of the charge neutrality level or branch point energy concept. The fifth method involves directly determining the VBO where distinct valence band maximum photoemission onsets can be discerned in valence band photoemission spectra. We will briefly review all five approaches here below.

The IP, i.e. the separation between the valence band maximum and the vacuum level, is determined by measuring the photoemission secondary electron cutoff and valence band maximum with respect to the Fermi level (figure 3). This is often done using ultraviolet photoemission which has the disadvantage of being extremely surface sensitive, leading to the possibility of characterizing the contamination on the surface of a material rather than the material itself. XPS can also be used, but extreme care must be taken to avoid saturating the photoelectron detector with the extremely high intensity of secondary electrons just before the secondary electron cutoff. Typically, this requires a reduction in the x-ray source power of a factor of around 20 [98] and can also involve narrowing of the electron analyzer slit width to reduce the intensity of photoelectrons reaching the detector. Many modern commercial XPS instruments do not allow these kind of measurements to be done to avoid damage to the electron detector when using normal operating settings.

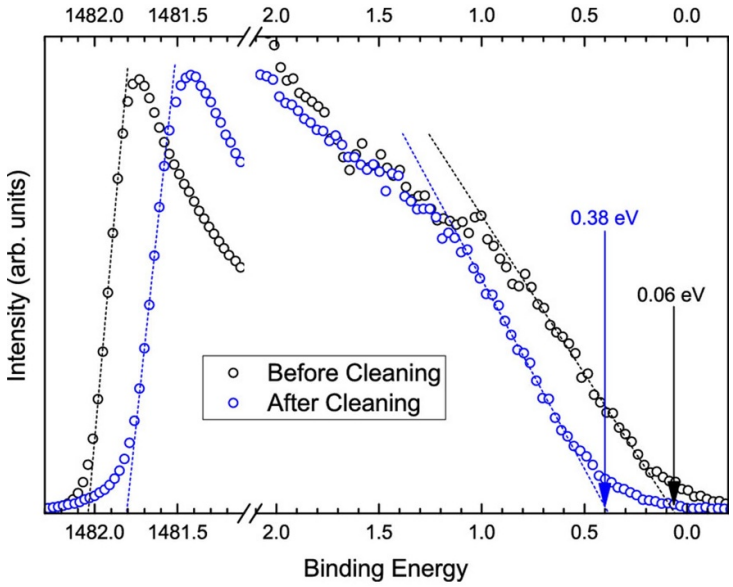

Figure 4. The secondary electron cutoff and valence band maximum of Cu_3BiS_3 recording using XPS ($h\nu = 1486.6$ eV) before and after cleaning using Ar ion sputtering. Reprinted and adapted with permission from [84]. Copyright (2019) by the American Chemical Society.

Using the terminology and labelling of figure 3, the ionization potential, IP, is given by

$$\mathrm{IP} = E_{\mathrm{vac}} - E_{\mathrm{VBM}} \tag{3}$$

where E_{vac} is the vacuum level and E_{VBM} is the valence band maximum of the material being investigated. The vacuum level is determined from

$$E_{\mathrm{vac}} = h\nu - E_{\mathrm{SEC}} \tag{4}$$

where $h\nu$ is the energy of the photon source and E_{SEC} is the secondary electron cutoff energy. Therefore,

$$\mathrm{IP} = h\nu - (E_{\mathrm{SEC}} - E_{\mathrm{VBM}}). \tag{5}$$

As it is conventional for photoemission spectra to be calibrated with respect to the Fermi level, care must be taken to ensure the correct sign is assigned to all quantities in order to obtain the correct IP value. Therefore, we illustrate IP determination with the following example, using the measurements of the SEC and VBM of Cu_3BiS_3 by XPS, after cleaning the surface, as shown in figure 4:

$$\mathrm{IP} = 1486.6 - 1481.8 + 0.38 = 5.18\ \mathrm{eV}. \tag{6}$$

This example also illustrates the significant impact that surface contamination can have on determined IP values, as before cleaning IP = 4.62 eV, indicating that surface oxides can play a role in band alignments and therefore in the operation of devices.

These photoemission measurements also determine the work function, the separation between the vacuum level and the Fermi level. The EA, the vacuum level to CBM separation, can also be determined either by subtracting the band gap of the material from the IP value obtained from optical spectroscopy or the literature or from inverse photoemission measurements of the CBM from the onset of unoccupied states. Care must be taken when using IPES, as its resolution is relatively low compared with UPS and monochromated XPS. Once the IP of different materials is known, their band alignment with respect to the Fermi level and therefore each other can be plotted as shown in figure 5 for Zn_2SbN_3.

While the natural band alignment is a good starting point in deciding device structure, a more thorough understanding of the device interface is often needed. The first step beyond natural band alignments from IPs is to use Anderson's rule [105, 106] which is also known as the EA rule. The Fermi levels of the two materials are aligned while the difference in the EAs at the interface is maintained from the natural alignment measurements. Charge transfer between the two materials is still neglected, as are crystallographic orientation or interface induced gap states that may form upon contacting the two materials. As a result, this approximation could deviate significantly from the real alignment of the bands [107, 108]. How the band

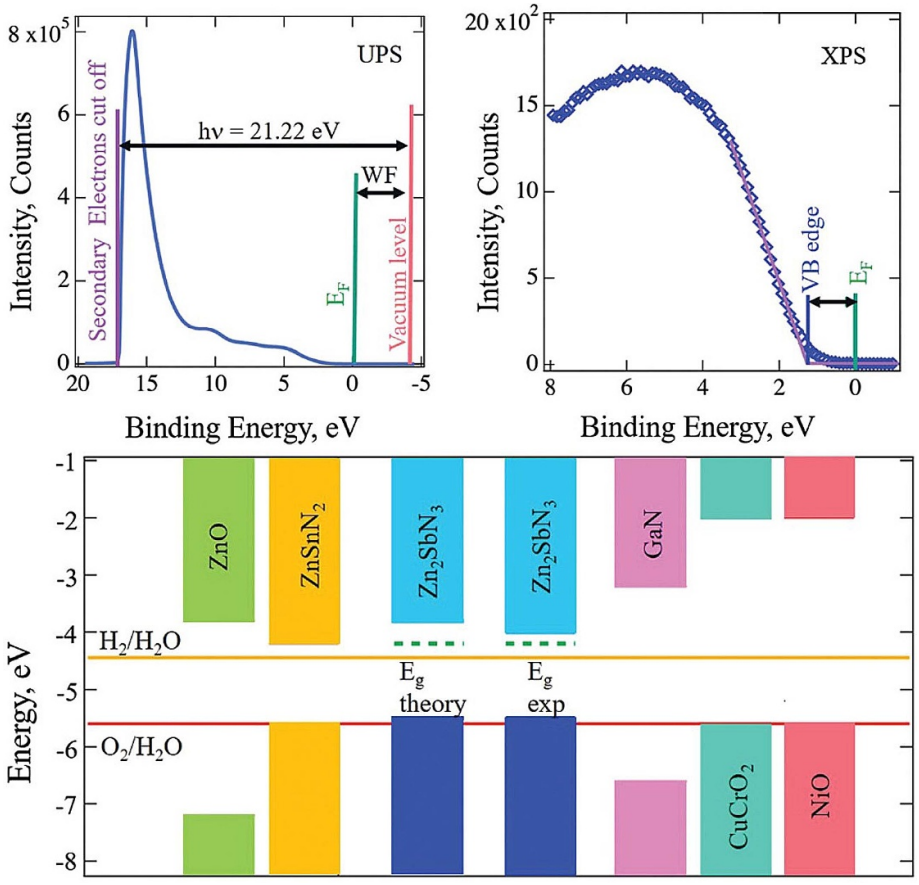

Figure 5. Experimental determination of how to derive natural band alignment of a given material, in this case Zn_2SbN_3. The determined IP is used to align the material's band edges with respect to the vacuum level as shown in c along with the band alignment of other related materials and the water redox potentials. Reproduced from [100] with permission of The Royal Society of Chemistry.

bending is divided between the two sides of the interface also has to be assumed or determined from complex additional measurements.

Band alignments between different materials can also be determined by plotting band edges with respect to the so-called charge neutrality level [109, 110] which has also variously been referred to as the branch point energy of the virtual gap states [111–113] and the Fermi level stabilization energy [114, 115]. This level is suggested to have a universal alignment for different materials and therefore can be used to determine the band alignment between materials. It is also associated with the $\epsilon(\pm)$ transition levels for interstitial hydrogen configurations which involve disrupting the cation-anion bond [116, 117].

Another method of estimating band alignment between materials is the so-called transitivity rule. If the band alignments between materials A and B and also B and C are known, then the alignment between A and C can be approximated from the other two alignments. This can provide a good initial estimate, but there is no substitute for experimental and theoretical determination of the band alignment from the interface VBO between the two materials themselves. The theoretical approach to this is described in section 4. The experimental approach once again employs photoemission spectroscopy, but now following an approach developed in the early 1980s by Kraut *et al* [118, 119], which has become known as the Kraut method.

The Kraut method employs photoemission measurements of a set of three samples to determine the VBO between two different materials, A and B: a 'thick' film of material A, a 'thick' film of material B and 'thin' film of A grown on B. Here, 'thick' means thick enough so that photoelectrons emitted from beneath the film being measured will all be inelastically scattered without leaving the material and entering the analyzer—for XPS, this means 20 nm or thicker. And 'thin' means thin enough that photoelectrons from material B can pass through material A and so to be detected by the electron analyzer—for XPS, a film thickness of about 5 nm is ideal for the 'thin' film. It is also important to make sure that the 'thin film' is a continuous closed layer. The property which determines the required 'thinness' of this film is the inelastic mean free path of the photoelectrons emitted from the material. This varies according to properties of the material and is strongly a function of the kinetic energy of the photoelectrons. It typically varies from 0.2 nm for low kinetic energy

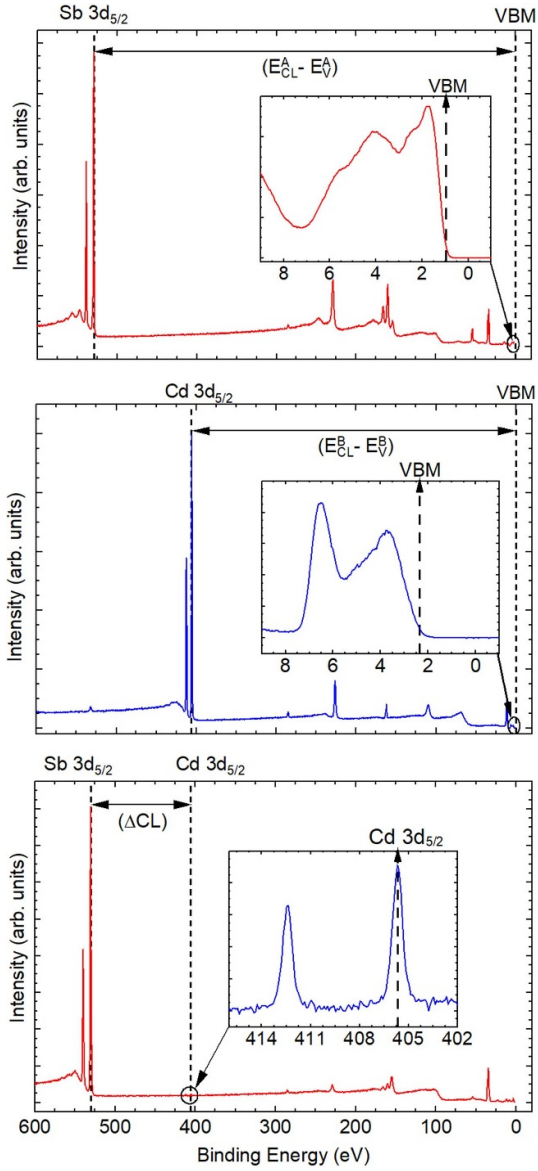

Figure 6. HAXPES measurements for Kraut method determination of the VBO between solar absorber Sb_2Se_3 and window layer CdS. The separations depicted in each of the three spectra correspond to the three terms in equation 7. Reproduced from [99]. CC BY 4.0.

(high binding energy) core levels to as high as 3 nm for high kinetic energy (low binding energy) core levels. The IMFP values corresponding to different core levels of a particular material for a given excitation source can be straightforwardly calculated using the TPP-2M method [120] using NIST's freely available code [121]. As it uses an actual interface between the two materials, the Kraut method accounts for the charge transfer across the interface, a phenomenon that is neglected by the other approaches discussed above.

In the Kraut method, the VBO, ΔE_V, between materials A and B is given by

$$\Delta E_V = (E^B_{CL} - E^B_{VBM}) - (E^A_{CL} - E^A_{VBM}) + \Delta E_{CL} \quad (7)$$

where E^A_{CL} and E^A_{VBM} respectively denote the binding energy of the core level and the valence band maximum of the 'bulk' material A with the same applying to material B and ΔE_{CL} is the separation between the same core levels from material A and material B, but in the data from the 'thin' film of A on B (see figure 6). This constitutes an abrupt interface approximation in which interface band bending is neglected. One other limitation of this method is that the growth of a representative film of material A to a thickness of only 5 nm can be difficult, depending on the material and its deposition method. This can be overcome by using HAXPES where synchrotron radiation or the recently developed lab-based sources [122, 123] can be used to give photon energies typically in the 5–9 keV range. While this has the drawback of reducing the photoionization cross section, this limitation is overcome by the greater photon intensity delivered by

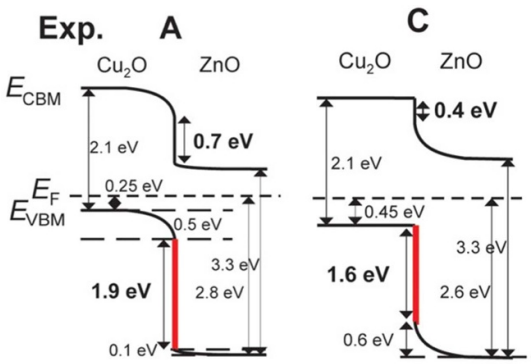

Figure 7. An example of the effect of the growth conditions on the band-bending of a give absorber/window layer. Reprinted and adapted with permission from [125]. Copyright (2016) by the American Chemical Society.

synchrotron sources. This results in an increase of the IMFP of the photoelectrons by a factor of 3 or 4, enabling films of up to ∼20 nm thickness to be used in VBO measurements using the Kraut method [99].

Further this method allows to assess further complications can arise depending on the growth conditions used to deposit both the absorber and the window layer. This is because, depending on the deposition conditions, formation of different defects can occur at the interface and thus different amounts of band bending or deleterious Fermi level pinning can be induced for a give pair of materials [124]. These was exemplified, for example, in the case Cu_2O/ZnO [125] and Cu_2O/ITO [126] band alignment. Pinning of the Fermi level at the interface occurs, but the position where the Fermi level is pinned and the different amount of band bending occurring at the interface is heavily dependent on the growth conditions even for the same pair of materials as shown in figure 7. Furthermore, formation of spurious phases can significantly reduce the achievable device performance even for materials with good bulk properties. For example, XPS measurements at the Cu_2O/ZnO interfaces shows that the growth conditions for ZnO (A and C) should be carefully selected in order to achieve a stoichiometric interface (i.e. Cu_2O) and prevent the formation of competing phases (Cu or CuO) [125] at the interface which will significantly reduce the open circuit voltage. On the other side, formation of Mg-$(Mg_xZn_{1-x})_2P_2$ spurious phase at the interfaces between Mg and Zn_2P_3 Schottky junctions was reported as contributing factor helping rectification at the interface [127, 128]. Yet the concomitant degradation of the interface with formation of voids and metallic by-products as well as the low carrier concentration in the Mg-$(Mg_xZn_{1-x})_2P_2$ layer which limits the achievable V_{OC} are key factors in hampering the performance of this material [128]. Interestingly, Zn_2P_3 is one such material where attempts to make heterojunctions resulted in devices with lower performance than the Mg-based Schottky diode, even for a configuration where the alignment at the interface leads to carrier-selective contacts [129]. In such cases, the good alignment at the interfaces is reflected directly with the improved V_{OC}, which however is largely counterbalanced by the loss from reduced short circuit current (J_{SC}). The physical cause for the significant decrease in the short circuit current density (J_{SC}) is unclear, but ultimately this results in low cell performance despite the originally very promising properties of the bulk material and an optimized band alignment.

$ZnSnN_2$ is one example of material for which both bulk properties and alignment at the interfaces needed to be optimized in order to achieve measurable device efficiency. Initially, this materials was unsuited for PV application due to the high carrier concentration, which was rendering it degenerately n-type in the *as deposited* formed. Over the past decade, progress was made in making the material semiconducting by optimizing growth conditions and off stoichiometry [40–43, 61, 91, 130]. The resulting defect chemistry is however rather complex, having to deal with both disorder in the cation sub-lattice, cation off-stoichiometry and presence of impurities such as oxygen, which are hard to avoid during deposition [130–132]. All these parameters play a complex role in defining the optoelectronic properties of the material having an effect on the magnitude of the band-gap, position of the band edges and carrier dynamics [43, 90, 91, 132]. The effect of these materials' properties on the formation of deep-levels (recombination centers) and minority carrier dynamics (recombination and scattering) is yet to be clarified. Natively n-type, $ZnSnN_2$ would hardly ever be p-type, even after extrinsic doping [102]. Thus, a heterojunctions approach is required for device applications. The first measurable devices were reported in 2018 [133], having SnO as the junction partner. However, the interface barrier and particularly the CBO was rather unfavorable for carrier extraction. Improvement in the device performance was obtained by adding a thin buffer layer, Al_2O_3, which was claimed to provide better passivation of the SnO and improve charge-selectivity at the contacts [62]. It has to

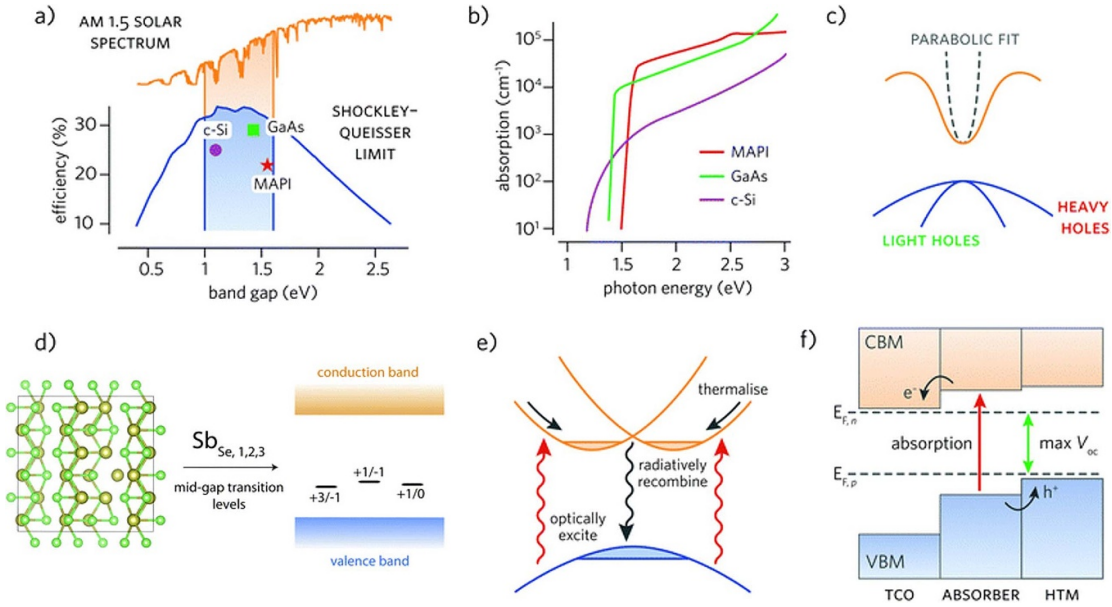

Figure 8. Properties of a solar absorber that are now readily calculable using computational approaches, including (a) band gap (Reproduced from [10]. CC BY 3.0), (b) optical absorption (Reprinted with permission from [139]. Copyright (2014) American Chemical Society), (c) band edge effective masses and thus mobilities, (d) defect chemistry (Reproduced from [140]. CC BY 3.0), (e) recombination and carrier capture (Reproduced from [141]. CC BY 4.0) and (f) band offsets.

be noticed that SnO is a weak absorber itself, thus further studies would be required to establish where the depletion region is located. In the outlook of potential earth-abundant nitride-based semiconductor, Zn_2SbN_3 might be a better option than $ZnSnN_2$. The material is natively semiconducting, without the strict requirements for off stoichiometry or post-annealing treatments to reduce the carrier concentration, PL-active already in a non-optimized form and possesses slightly higher valence band and conduction band edges than for $ZnSnN_2$ [100]. Devices comprising this material have yet to be made.

The importance of interfaces is not just limited to improving device efficiency but it might play a major role in terms of device stability too. Schultz *et al* have recently reviewed in detail the role of interfaces in the degradation mechanism for perovskite solar cells, highlighting the specific challenges of experimental characterization of the perovskite solar cells [134] and the role of interfaces in the overall stability [11]. The reader is referred to their papers for more information on the subject.

Experimental determination of band alignment at the interface has had a tremendous role in understanding charge transfer at the interface and guiding the device optimization process. The method is undeniably time-consuming, and with the advent of modern computational methods, determination of vacuum levels or band alignment exclusively based on experimental approaches has become rarer. Recent papers often make a use of a combination of both spectroscopy and theoretical calculations, with the mutual benefit of validating the theoretical calculations based on a correct reproduction of the band edge features and a fast determination of the theoretical natural band alignment which can guide the experimentalist on a fast track for device optimization. Discussion of this complementary approach with both advantages and disadvantages is reported in the following section.

4. Integrating x-ray photoelectron spectroscopy and DFT calculation

With the advent of modern computing, theoretical and experimental approaches have become more and more complementary, contributing to the fast development of materials. In the field of emerging solar absorbers, this complementary approach span from the understanding of the basic properties of the materials, to the design of new materials that might have the desired chemical and physical properties up to device physics understanding and optimization (figure 8). Thus DFT has progressed from understanding basic materials properties after the fact, in other words, after the experimental synthesis of the new materials, to a more predictive role, in terms high-throughput materials discovery. Using DFT, an expert user can now routinely calculate the electronic structure, band structure and optical absorption spectra of any potential solar absorber. Going beyond models of non-defective crystals, however, is much more computationally expensive, but if willing to pay the computational cost, one can now predict the defect chemistry of a candidate solar absorber. This is a fundamental contribution to the field of photovoltaics, as it allows the

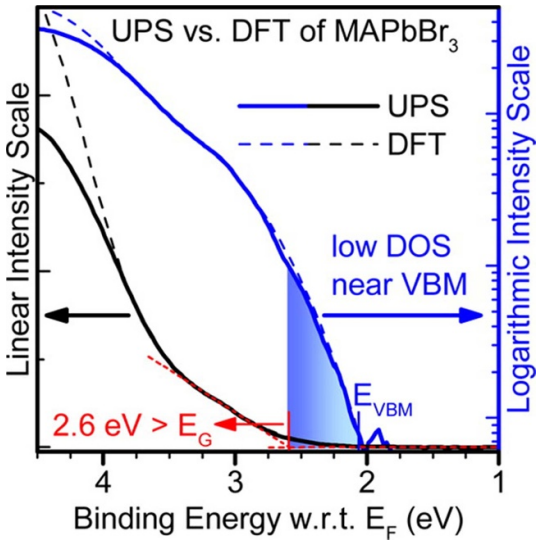

Figure 9. Comparison between experimentally determined density of states and the correspondent DFT calculations. Reprinted and adapted with permission from [163]. Copyright (2016) by the American Chemical Society.

determination of how tolerant a materials is to defects, and when it is not, it provides useful insights into what growth conditions should be used to avoid their deep defect formation. Worth emphasizing is a recent perspective by Zunger and Walsh on how 'instill' defect tolerance in materials that are not necessarily such, by engineering doping and presence of impurities to manipulate the presence and position of electronic levels in the band gap [13]. Whereas widely used, defect calculations are more computationally expensive and thus far, high-throughput calculations of defects is a subject in its infancy in comparison to the more established frameworks for materials predictions [135, 136]. These in part because defect calculations requires additional post-DFT corrections to account for the effect of the errors in the band-gap prediction on defect electronic levels, finite size of the computational cell, correct definition of the chemical potential for metastable materials [135–138] etc. Certainly this is an area for growth. At the same time, the ability to calculate surface terminations of materials and interfaces, led to the development of computational capabilities to support the device-fabrication aspect of PV technologies, by identifying device architectures that maximize carrier extraction. The advantages and limitations of these approaches will be reviewed in details in this section.

In terms of basic materials properties, a large fraction of the theoretical efforts in the last decade was devoted to understanding the origin of *defect tolerance*, and once some of the principles were understood, in trying to design materials that replicate those properties. Initial studies determined that the Pb $6s^2$ configuration was a key-aspect to lead to defect tolerance [9, 10] in MAPI. As a result new or already known materials comprising elements such as Sb^{3+} or Bi^{3+} received particular attention. This included compounds such as Sb_2S_3 [142–146], SbSI [147, 148], BiI_3 [149–152], BiSI [153, 154], BiOI [93, 96, 155]. Solar cells comprising these materials only show efficiency of few percentage, with exception of Sb_2S_3 whose efficiency raised from 7.5% in 2014 [146] to 9.2% in 2019 [156] and $Sb_2(S,Se)_3$, which has a reported 10.5% efficiency in 2020 [157, 158]. Although this moderate success is undeniable, none of these materials is actually *defect tolerant*. Quite contrary, often times their defect chemistry is quite complex, with mid-gap states present for almost all of them [159, 160]. By now, it has become clearer that it is the concomitant existence of several physical properties in hybrid-perovskite which leads to the final macroscopic effect of *defect tolerance*. In addition to the favorable Pb $6s^2$ configuration, physical properties that contribute to the defect tolerance are the smaller capture cross-section due to the high dielectric constant of the material [57] and the crystallographic structure [57, 161]. In cubic perovskite the lone-pair s-electrons strongly interact with the anions p-electrons giving rise to a highly disperse valence band maximum and result in the latter being high in energy [162]. Moreover, the structure favors a strong coupling between the cation s-levels and the anion p-levels thus giving rise to strong antibonding characters of the band edges [162]. Crystal structures that disfavor these interactions usually leads to materials with much lower PV properties [162]. The antibonding nature of the VB and the low value of IP both contributes to achieve shallow level type of defects, particularly for vacancy-type of defects [57]. Comparison between theoretically calculated and experimentally measured density of states for both valence band (XPS/UPS) (figure 9) and conduction bands (IPES) validated the basis of this theory, showing an excellent agreement with the composition and dispersion of the band edges calculated by DFT, as well as the absence of substantial defects states in the gap [163].

The knowledge build by these studies has contributed to establish designing principle for the discovery of materials, which could possess at least some of these features, creating a wave of new solar absorbers [10, 57, 153, 162, 164, 165]. The problem remains about translating these materials into highly performing devices or contrary, to identify unsurmountable bottlenecks at the very beginning.

In recent years, the continued development of high-performance computing capabilities has meant that the calculation of very accurate electronic structures for candidate PV materials using first principles approaches has become possible. Computational photoemission spectra can be calculated using advanced techniques such as the GW approach which comes in many computationally expensive flavors in open source codes such as the YAMBO code [166]. A very accurate GW approach is the quasiparticle self-consistent GW method (which for example is available in the QUESTAAL code [167]) and yields electronic structures in excellent agreement with experiment [168]. These GW approaches represents the 'gold standard' for electronic structure analysis for solids, however, this comes with a significant computational cost, and is not generally attempted for unit cells with a large number of atoms, or for defective supercells. A full explanation of GW theory is beyond the scope of this review, however, interested readers are pointed towards an excellent overview from Rinke *et al* and related references therein [169].

In cases where the direct calculation of photoemission spectra is not possible, standard DFT and hybrid-DFT approaches can be used to calculate the electronic structure of the material of interest, using a plethora of DFT codes including proprietary codes such as the Vienna *Ab Initio* Simulation Package [170, 171], the CAmbridge Serial Total Energy Package [172] and the Fritz Haber Institute *ab initio* molecular simulations package [173], or open source codes such as Quantum ESPRESSO [174] or GPAW [175]. A thorough description of the many flavors of DFT is also beyond the scope of this review, however interested readers are encouraged to read some of the many books on electronic structure theory [176, 177].

The calculated partial density of states can be weighted according to the photoionization cross sections of the atoms involved, taking the energy of the radiation source used and the experimental broadening into account, and this can generate a simulated XPS/UPS/HAXPES spectra [178]. These simulated spectra can then be directly compared to the experimental measurements, allowing validation of structure-property relationships [85, 122, 179, 180].

To provide insight into the band edges (ionization potential, IP and electron affinity, EA) of candidate PV absorbers versus the vacuum level, the standard computational approach is to create a slab model in a periodic DFT code [181]. This involves the construction of a 2D slab, with a portion of the cell containing the crystal structure of interest, terminated by a certain Miller index termination, with the rest of the cell comprising a vacuum. This requires large separation between slabs, typically 15–30 Å (this is material dependent and should be check for convergence). The electrostatic potential should plateau in the vacuum space, as seen in figure 10(a), and while the slab valence band energy is not meaningful due to the presence of the surface termination, this plateau can be compared in energy to the energy of a chosen core state on an atom that is deep in the slab, to approximate 'bulk-like' behaviour. Using the core-level alignment method developed by Wei and Zunger [101], the vacuum-core level separation can then be compared to the VBM-core level separation from the bulk calculation to obtain the vacuum-VBM separation, which is the IP of the bulk:

$$\mathrm{IP} = E_{\mathrm{vac}} - E_{\mathrm{VBM,\,bulk}} = (E_{\mathrm{vac}} - E_{\mathrm{core,\,slab}}) - (E_{\mathrm{VBM,\,bulk}} - E_{\mathrm{core,\,bulk}})\,. \tag{8}$$

The position of the EA is then approximated by using the calculated band gap, E_{g}, using the relationship $E_{\mathrm{g}} = \mathrm{IP} - \mathrm{EA}$. In practice, the planar average of the electrostatic potential calculated by the electronic structure package can be extracted using the MacroDensity package produced by Butler *et al* [182, 183].

This approach has been used to rationalize the poor performance of earth abundant solar absorbers, such as SnS [97] and more recently for BiSI [153].

In the case of SnS, it has been suggested that poor band alignment is most likely the reason for the poor devices performance [97, 184]. This is due to the unusually low value of IP for being a p-type semiconductors, which leads to an interface mismatch between the absorber and one of the most commonly used n-type junction partners, CdS [97, 184]. Comparison between theoretically and experimentally determine Valence band maximum reveals that the origin of such low value of IP span from electronic structure of the materials, specifically the hybridization of Sn 5s lone pair with the cation (Sn) 5p levels and the anion (S) 2p levels [98]. The lone-pair states result in the raise of the position of the Valence Band Maximum of the material with respect to vacuum and hence a lower IP than what normally observed in p-type materials [98]. As a result, the CdS contact layer, which might work for materials with high value of IP, will not produce a good band-alignment for materials with a low IP.

BiSI solar cells were fabricated by Hahn *et al* using p-CuSCN and FTO as the hole and electron transporting layers respectively, which had a PCE of only 0.012% [154]. Calculation of the IP and EA for BiSI

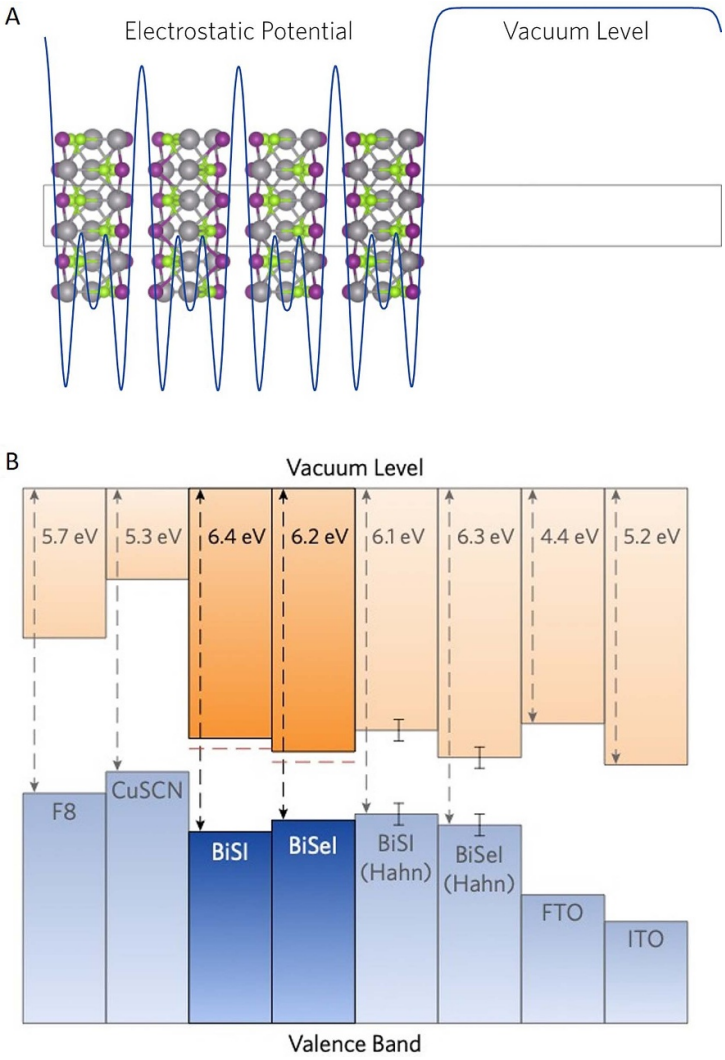

Figure 10. (a) 2D slab model of BiSeI used to align the electronic eigenvalues to the vacuum level viewed along the [010] direction. The corresponding electrostatic (Hartree) potential calculated using HSE06 is shown in blue. Bi, Se, and I atoms are denoted by grey, green, and purple spheres, respectively. (b) Calculated band alignment of BiSI and BiSeI versus a range of hole and electron transport layers, taken from. Reproduced from [153]. CC BY 3.0.

(figure 10(b)), however, indicated that the IP was unexpectedly large, at 6.4 eV, meaning that the VBM of CuSCN was only ∼0.4 eV below the CBM of BiSI, placing a limit on the possible open circuit voltage. Due to these computational insights, Poly(fluorine-2,7-diyl, also known as F8), was suggested as an alternative hole transporting material, and last year this prediction was validated when Tiwari *et al* used F8 as a hole transport layers to increase the PCE of BiSI cells to 1.32% [185]. It should be noted that this approach represents a first approximation for determining band alignments of cell layers, and does not include any interface effects.

More recently, in the case of the enargite (Cu_3AsS_4) and bournonite ($SuPbSbS_3$) minerals, Walsh *et al* have married IP and EA with lattice constant matching to predict partner layers that could also minimize strain and achieve epitaxy [104]. Taking band edge data from 173 measured or calculated IPs from [186] and the ElectronLatticeMatch Library [187], this approach predicted that candidate partner materials included SnS_2, ZnTe, WO_3 and Bi_2O_3.

The most computationally costly approach to finding efficient junction partners is to explicitly calculate the interface between the absorber and the transport layers. This can be relatively straightforward when the layers are of the same structure type [188]. When the crystal structures are very different, then this becomes quite a bit more complex. Patrick and Giustino, having no *a priori* information on the interface between Sb_2S_3/Sb_2Se_3 and anatase TiO_2, were forced to use three assumptions when generating their interface model: (a) that the Sb_4S_6 ribbons would absorb parallel on the anatase (101) surface, (b) that anatase and Sb_2S_3 are lattice matched along the direction of the Sb_4S_6 ribbons, and (c) the (101) anatase termination is not defective [189]. Nevertheless, their model pointed to Sb_2Se_3 being a better photosensitizer than Sb_2S_3, which has been now experimentally realized.

To truly understand a complex interface, one must consider using crystal structure prediction to build up an atomic picture of the interface between two dissimilar materials. This approach is highlighted by the study of Zhu *et al* on the interfaces between $SrTiO_3$ and CeO_2 [190]. In this work, the authors have used an interatomic potential approach to cut down on the computational cost of searching all potential interfaces, however they do use DFT to verify the stable nature of the predicted interfaces. This approach yielded previously unknown structure, which were more stable than that of interfaces that have been hand built.

Therefore, the ability to computationally guide the experimental design of PV devices is improving, and improvements in computational power are making the analysis of interface effects a more regular occurrence. In the not too distant future, it will be possible to predict the optimum device architecture for a new absorber based solely on computational analysis to enable the time-consuming and often costly device fabrication and characterization experiments on a more focused, better defined path. As for now, a complementary approach with (a) a good theoretical understanding of the defect chemistry of a given materials that could help experimentalist choose synthetic condition to disfavor the formation of deep defects, (b) an understanding of both experimental and theoretical natural band alignment to choose junction partners, instead of following the so often misleading road of adopting parental device structure and (c) an understanding of the chemical stability of the interface by experimentally probing the interface through photoelectron spectroscopy methods, appears to be the most rational and successful approach to follow. The further development from an experimental standpoint of in-operando device characterization represent the next generation of device characterization and development, where the bottleneck of device components and fabrication steps can be identified and addressed based on the characterization of the device output characteristics.

5. In-operando methods

A very powerful tool for the development of solar absorbers is represented by the use of the *in-operando* characterization techniques. The *in-operando* methods for characterization of solar absorbers developed almost in parallel for PV applications and PEC applications. In terms of PV applications it is possible to determine the V_{OC} of a solar cell by x-ray photoelectron spectroscopy [48]. *In-operando* methods for PEC applications, largely benefited from the development of near ambient pressure photoelectron (NAP-XPS, also known as AP-XPS) at synchrotron facilities [191–194], and further progress into lab-based NAP-XPS system becoming widely available [194, 195]. In this case, most of the studies focused on the electrochemical aspect of the devices [196, 197], while rarely discussing the effect of light-bias [198]. Here we discuss the advantages of *in-operando* methods applied to PV systems and how this method could be further extended to the PEC application to complement the already existing suite of *in-operando* characterization methods.

In relation to PV application, the direct measurement of the Fermi level splitting achievable in a given absorber after passivation [48] was reported in 2016. To explain this method, we will take into consideration the simplest case of a p–n junction, e.g. Cu_2O/ZnO deposited on glass. In order to measure the Fermi level splitting, the sample should consist of a passivated absorber, for example a junction pair, and the amount of Fermi level splitting will be determined as the difference between a given core-level recorded in dark vs illumination. The technique is extremely simple but requires care in mounting the sample. The first step consist in measuring the junction in dark. The correct way to do this is to shorten both back and front contact as shown in figure 11(b). The reason for this is that even the very low amount of light coming from an ion-gauge or the x-rays themselves are enough to induce an appreciable amount of photo-voltage in a well-passivated material if this is simply connected to ground as shown in figure 11(a) (dark). When the sample is mounted as shown in figure 11(b), the Fermi levels of the absorber and its junction partner, are aligned and both connected to ground. We will call the core-levels recorded under these conditions a 'true dark'. In order to measure the quasi-Fermi level splitting, the top surface should be left floating and only the bottom electrode should be contacted to ground as shown in figure 11(a). Prior to starting the measurements and under no illumination, the Fermi levels are still aligned but only the absorber is connected to ground. Upon illumination, the Fermi level splitting occurs, with the absorber, in our case Cu_2O, resting at the quasi-Fermi level for holes which is at ground potential, whereas the top layer, in our case ZnO, is resting at the quasi-Fermi levels for electrons. This means that the core-levels for ZnO in this case are shifted to a lower Binding Energies by an amount equal to the *quasi-Fermi* level splitting (hence the qV_{OC} in the device) in comparison to the same core-level recorded under dark.

The caveat of the technique is that the contact materials (e.g. ZnO) should not have a strong surface photovoltage, which might interfere with the measurements itself. The presence of this potential issue can be easily determined by measuring a reference sample, in this case the ZnO layer directly deposited on glass for example, both under dark and under illumination. If no surface photovoltage is present, core levels of this reference sample recorded under light and under illumination will superimpose. Another method to exclude x-ray induced surface photovoltage is to measure the reference sample (ZnO deposited on glass in this

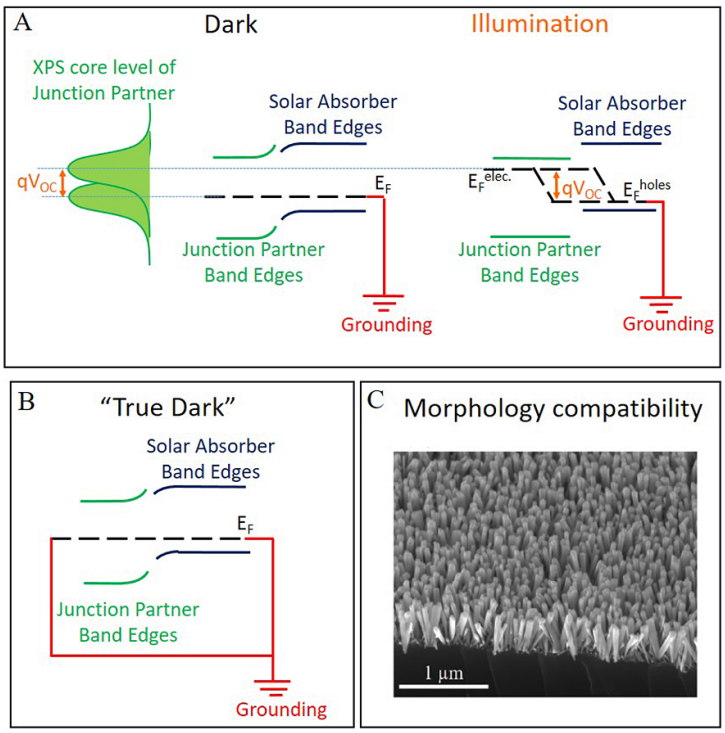

Figure 11. (a) Schematics of the in-operando measurements for PV absorbers under dark and under illumination; (b) because the x-ray and any stray light might induce already photovoltage, the front contact and the absorbers need to be shorted in order to prevent the onset of any quasi-Fermi level splitting. An example of the morphologies to which the method has been applied: the non-contact nature of the method makes it suitable to nanowires devices such as those reported in figure (c). Reprinted and adapted with permission from [199]. Copyright (2018) by the American Chemical Society.

example) as a function of x-ray power. If surface photovoltage is present, the core level will shift as a function of x-ray power. In the case of a surface photovoltage being present, this needs to be taken into account when drawing the band alignment as reported in [48].

This technique is rather powerful and represents a direct method to measure quasi-Fermi level splitting (and thus the qV_{OC}) without the need to build a full device-stack. This means that the technique can be applied for example for the screening of potential contact materials or to assess how deposition of subsequent layers affect the obtainable V_{OC}. It is worth emphasizing that this effect should be taken into account when measuring band alignment if the sample is mounted as in figure 11(a). As previously mentioned, x-ray power and stray light present in the chamber could induce a measurable photovoltage already, and thus the band alignment drawn without taking into account this effect could be erroneous [34]. It is thus recommended that, when measuring the band alignment of the interface using the methods described in section 3 of this review, the presence of a photovoltage is assessed. A quick test to determine if this effect is present while measuring the band alignment is to acquire spectra at different x-ray power.

Another advantage of this technique is its contactless nature, which makes it amenable to non-planar structures. This mean that the technique can be applied not only to thin films PV devices, but also to nanowire solar cells and PEC devices, thus complementing the *in-operando* techniques already developed for PEC applications. In particular, materials such as Sb_2S_3 [200] and BiOI [201] which have both been considered for PV and PEC application, will largely benefit from combining the in-operando methods, particularly for devices which suffers from severe V_{OC} deficit [200].

6. Conclusions and outlook

In this review we have outlined the progress made in the field of photoemission spectroscopy and DFT calculations to accelerate the development of new solar absorbers for photovoltaics applications.
In summary, for a prospective new solar absorber, the first decision often is based on whether the materials have a high minority carrier lifetime, which could lead to efficient extraction of the photo-generated carriers. However, care needs to be taken when estimating this quantity for new materials, as many of the parameters required to determine the minority carrier lifetime are often unknown and artifacts can lead to an overestimation of this quantity. In many cases the rule of thumb is set at minority carrier lifetime exceeding

1 ns. Further, DFT has been a powerful tool in helping to understand if a material has the potential to have favorable bulk defect chemistry, i.e. formation of shallow defects only, under given depositions conditions. This property, often named 'defect tolerance', has been largely satisfied in hybrid perovskite materials, at the cost however, of severe limitation in terms of stability.

If and when these conditions are met, the second step is normally the fabrication of a device. In many instances, the first approach is to adopt a device layout used for traditional absorbers. Although tempting, this might not represent the most efficient avenue, as in many cases this has led to poor band alignment at the interfaces and thus low-performing devices. Both theoretical and experimental methods could help in making better choices by using the natural band alignment as a first selector of a junction partner. This has to be followed by direct measurements of the band alignment at the interface for the given deposition conditions used for the device fabrication by XPS. Indeed, different growth environments and deposition methods can introduce a variable amount of defects in the bulk and at the interface of the materials under investigation, which can lead to a rapid deterioration of the device performance if the interface energetics are not optimized. In recent years, much progress has been made in terms of adapting this technique to *in-operando* conditions, for application of absorber materials both in the PV and PEC field.

The *in-operando* PV techniques have been so far mostly applied to established technologies; however this could be an extremely powerful tool to accelerate the development of new materials by for example, applying it as a screening method to select suitable junctions' partners. This approach will immediately correlate the usefulness of a potential partner materials to the device output characteristics without the need to build a full device-stack. Additionally, this technique could help to narrow down the fabrication step responsible for degradation of the device properties. Similarly, the PEC field will greatly benefit from merging the *in-operando* techniques developed to characterize the electrochemical part of the process, to the technique developed for the PV application, thus enabling the characterization of the photo-electro-chemical processes.

Overall, the challenges of developing new solar absorbers that could meet or exceed the performance of established technologies, both in terms of efficiency and stability, are far from trivial. For this reason, synergist approaches bridging theory and experiments that can unravel the interplay between bulk—interface—device properties and the ability to correlate them to the fabrication processes are required.

Acknowledgments

This work was supported by the US Department of Energy's Office of Energy Efficiency and Renewable Energy (EERE) under Solar Energy Technologies Office (SETO) Agreement No. 34324. TDV acknowledges support from the Engineering and Physical Sciences Research Council (EPSRC), UK (EP/N015800/1) and helpful discussions with Huw Shiel. DOS acknowledges support from the EPSRC (EP/N01572X/1) and from the European Research Council, ERC (Grant No. 758345). TDV and DOS acknowledge membership of the Materials Design Network.

ORCID iDs

Tim D Veal https://orcid.org/0000-0002-0610-5626
Elisabetta Arca https://orcid.org/0000-0003-0651-6000

References

[1] Haegel N M *et al* 2019 Terawatt-scale photovoltaics: transform global energy *Science* **364** 836–8
[2] Butler D 2008 Thin films: ready for their close-up? *Nature* **454** 558–9
[3] Powell D M, Winkler M T, Choi H J, Simmons C B, Needleman D B and Buonassisi T 2012 Crystalline silicon photovoltaics: a cost analysis framework for determining technology pathways to reach baseload electricity costs *Energy Environ. Sci.* **5** 5874–83
[4] Dhere N G 2007 Toward GW/year of CIGS production within the next decade *Sol. Energy Mater. Sol. Cells* **91** 1376–82
[5] Lee T D and Ebong A U 2017 A review of thin film solar cell technologies and challenges *Renew. Sustain. Energy Rev.* **70** 1286–97
[6] Polman A, Knight M, Garnett E C, Ehrler B and Sinke W C 2016 Photovoltaic materials: present efficiencies and future challenges *Science* **352** aad4424
[7] Liu F, Zeng Q, Li J, Hao X, Ho-Baillie A, Tang J and Green M A 2020 Emerging inorganic compound thin film photovoltaic materials: progress, challenges and strategies *Mater. Today* **41** 120–42
[8] Brandt R E *et al* 2017 Searching for 'defect-tolerant' photovoltaic materials: combined theoretical and experimental screening *Chem. Mater.* **29** 4667–74
[9] Brandt R E, Stevanović V, Ginley D S and Buonassisi T 2015 Identifying defect-tolerant semiconductors with high minority-carrier lifetimes: beyond hybrid lead halide perovskites *MRS Commun.* **5** 265–75
[10] Ganose A M, Savory C N and Scanlon D O 2017 Beyond methylammonium lead iodide: prospects for the emergent field of ns^2 containing solar absorbers *Chem. Commun.* **53** 20–44
[11] Schulz P, Cahen D and Kahn A 2019 Halide perovskites: is it all about the interfaces? *Chem. Rev.* **119** 3349–417

[12] Walsh A, Scanlon D O, Chen S, Gong X G and Wei S-H 2015 Self-regulation mechanism for charged point defects in hybrid halide perovskites *Angew. Chem.* **127** 1811–4
[13] Walsh A and Zunger A 2017 Instilling defect tolerance in new compounds *Nat. Mater.* **16** 964–7
[14] Yang D, Lv J, Zhao X, Xu Q, Fu Y, Zhan Y, Zunger A and Zhang L 2017 Functionality-directed screening of Pb-free hybrid organic–inorganic perovskites with desired intrinsic photovoltaic functionalities *Chem. Mater.* **29** 524–38
[15] Hoye R L Z *et al* 2017 Perovskite-inspired photovoltaic materials: toward best practices in materials characterization and calculations *Chem. Mater.* **29** 1964–88
[16] Zakutayev A, Allen A J, Zhang X, Vidal J, Cui Z, Lany S, Yang M, DiSalvo F J and Ginley D S 2014 Experimental synthesis and properties of metastable $CuNbN_2$ and theoretical extension to other ternary copper nitrides *Chem. Mater.* **26** 4970–7
[17] Sun W *et al* 2019 A map of the inorganic ternary metal nitrides *Nat. Mater.* **18** 732–9
[18] Filip M R, Liu X, Miglio A, Hautier G and Giustino F 2018 Phase diagrams and stability of lead-free halide double perovskites $Cs_2BB'X_6$: b = Sb and Bi, B′ = Cu, Ag, and Au, and X = Cl, Br, and I *J. Phys. Chem.* C **122** 158–70
[19] Hinuma Y *et al* 2016 Discovery of earth-abundant nitride semiconductors by computational screening and high-pressure synthesis *Nat. Commun.* **7** 11962
[20] Zunger A 2018 Inverse design in search of materials with target functionalities *Nat. Rev. Chem.* **2** 0121
[21] Ludwig A 2019 Discovery of new materials using combinatorial synthesis and high-throughput characterization of thin-film materials libraries combined with computational methods *npj Comput. Mater.* **5** 70
[22] Gautier R, Zhang X, Hu L, Yu L, Lin Y, Sunde T O L, Chon D, Poeppelmeier K R and Zunger A 2015 Prediction and accelerated laboratory discovery of previously unknown 18-electron ABX compounds *Nat. Chem.* **7** 308–16
[23] Wang Q, Perkins J, Branz H M, Alleman J, Duncan C and Ginley D 2002 Combinatorial synthesis of solid state electronic materials for renewable energy applications *Appl. Surf. Sci.* **189** 271–6
[24] Zawadzki P, Baranowski L L, Peng H, Toberer E S, Ginley D S, Tumas W, Zakutayev A and Lany S 2013 Evaluation of photovoltaic materials within the Cu-Sn-S family *Appl. Phys. Lett.* **103** 253902
[25] Caskey C M, Richards R M, Ginley D S and Zakutayev A 2014 Thin film synthesis and properties of copper nitride, a metastable semiconductor *Mater. Horiz.* **1** 424–30
[26] Rühle S, Anderson A Y, Barad H-N, Kupfer B, Bouhadana Y, Rosh-Hodesh E and Zaban A 2012 All-oxide photovoltaics *J. Phys. Chem. Lett.* **3** 3755–64
[27] Anderson A Y, Bouhadana Y, Barad H-N, Kupfer B, Rosh-Hodesh E, Aviv H, Tischler Y R, Rühle S and Zaban A 2014 Quantum efficiency and bandgap analysis for combinatorial photovoltaics: sorting activity of Cu–O compounds in all-oxide device libraries *ACS Comb. Sci.* **16** 53–65
[28] Yosipof A, Nahum O E, Anderson A Y, Barad H-N, Zaban A and Senderowitz H 2015 Data mining and machine learning tools for combinatorial material science of all-oxide photovoltaic cells *Mol. Inform.* **34** 367–79
[29] Panigrahi S, Nunes D, Calmeiro T, Kardarian K, Martins R and Fortunato E 2017 Oxide-based solar cell: impact of layer thicknesses on the device performance *ACS Comb. Sci.* **19** 113–20
[30] Rühle S, Barad H N, Bouhadana Y, Keller D A, Ginsburg A, Shimanovich K, Majhi K, Lovrincic R, Anderson A Y and Zaban A 2014 Combinatorial solar cell libraries for the investigation of different metal back contacts for TiO_2–Cu_2O hetero-junction solar cells *Phys. Chem. Chem. Phys.* **16** 7066–73
[31] Welch A W, Zawadzki P P, Lany S, Wolden C A and Zakutayev A 2015 Self-regulated growth and tunable properties of $CuSbS_2$ solar absorbers *Sol. Energy Mater. Sol. Cells* **132** 499–506
[32] Baranowski L L, Zawadzki P, Lany S, Toberer E S and Zakutayev A 2016 A review of defects and disorder in multinary tetrahedrally bonded semiconductors *Semicond. Sci. Technol.* **31** 123004
[33] Chen C *et al* 2017 Accelerated optimization of TiO_2/Sb_2Se_3 thin film solar cells by high-throughput combinatorial approach *Adv. Energy Mater.* **7** 1700866
[34] Siol S, Schulz P, Young M, Borup K A, Teeter G and Zakutayev A 2016 Combinatorial *in situ* photoelectron spectroscopy investigation of Sb_2Se_3/ZnS heterointerfaces *Adv. Mater. Interface* **3** 1600755
[35] Zakutayev A, Caskey C M, Fioretti A N, Ginley D S, Vidal J, Stevanovic V, Tea E and Lany S 2014 Defect tolerant semiconductors for solar energy conversion *J. Phys. Chem. Lett.* **5** 1117–25
[36] Zakutayev A 2016 Design of nitride semiconductors for solar energy conversion *J. Mater. Chem.* A **4** 6742–54
[37] Extance A 2019 The reality behind solar power's next star material *Nature* **570** 429–32
[38] Correa-Baena J-P, Saliba M, Buonassisi T, Grätzel M, Abate A, Tress W and Hagfeldt A 2017 Promises and challenges of perovskite solar cells *Science* **358** 739
[39] Jaramillo R, Sher M-J, Ofori-Okai B K, Steinmann V, Yang C, Hartman K, Nelson K A, Lindenberg A M, Gordon R G and Buonassisi T 2016 Transient terahertz photoconductivity measurements of minority-carrier lifetime in tin sulfide thin films: advanced metrology for an early stage photovoltaic material *J. Appl. Phys.* **119** 035101
[40] Feldberg N *et al* 2013 Growth, disorder, and physical properties of $ZnSnN_2$ *Appl. Phys. Lett.* **103** 042109
[41] Fioretti A N, Zakutayev A, Moutinho H, Melamed C, Perkins J D, Norman A G, Al-Jassim M, Toberer E S and Tamboli A C 2015 Combinatorial insights into doping control and transport properties of zinc tin nitride *J. Mater. Chem.* C **3** 11017–28
[42] Fioretti A N, Stokes A, Young M R, Gorman B, Toberer E S, Tamboli A C and Zakutayev A 2017 Effects of hydrogen on acceptor activation in ternary nitride semiconductors *Adv. Electron. Mater.* **3** 1600544
[43] Veal T D, Feldberg N, Quackenbush N F, Linhart W M, Scanlon D O, Piper L F J and Durbin S M 2015 Band gap dependence on cation disorder in $ZnSnN_2$ solar absorber *Adv. Energy Mater.* **5** 1501462
[44] Kimball G M, Müller A M, Lewis N S and Atwater H A 2009 Photoluminescence-based measurements of the energy gap and diffusion length of Zn_3P_2 *Appl. Phys. Lett.* **95** 112103
[45] Wyeth N C and Catalano A 1979 Spectral response measurements of minority-carrier diffusion length in Zn_3P_2 *J. Appl. Phys.* **50** 1403–7
[46] Olsen L C, Addis F W and Miller W 1982 Experimental and theoretical studies of Cu_2O solar cells *Sol. Cells* **7** 247–79
[47] Bhushan M and Catalano A 1981 Polycrystalline Zn_3P_2 Schottky barrier solar cells *Appl. Phys. Lett.* **38** 39–41
[48] Teeter G, Harvey S P, Perkins C L, Ramanathan K and Repins I L 2019 Comparative operando XPS studies of quasi-Fermi level splitting and open-circuit voltage in CZTSe/CdS and CIGS/CdS junctions and device structures *J. Vac. Sci. Technol.* A **37** 031202
[49] Ding L, Harvey S P, Teeter G and Bertoni M I 2016 Operando XPS characterization of selective contacts: the case of molybdenum oxide for crystalline silicon heterojunction solar cells *2016 IEEE 43rd Photovoltaic Specialists Conf. (PVSC)* pp 3543–6
[50] Tress W 2017 Perovskite solar cells on the way to their radiative efficiency limit—insights into a success story of high open-circuit voltage and low recombination *Adv. Energy Mater.* **7** 1602358

[51] Steirer K X, Schulz P, Teeter G, Stevanovic V, Yang M, Zhu K and Berry J J 2016 Defect tolerance in methylammonium lead triiodide perovskite *ACS Energy Lett.* **1** 360–6
[52] Jena A K, Kulkarni A and Miyasaka T 2019 Halide perovskite photovoltaics: background, status, and future prospects *Chem. Rev.* **119** 3036–103
[53] Yin W-J, Shi T and Yan Y 2014 Unusual defect physics in $CH_3NH_3PbI_3$ perovskite solar cell absorber *Appl. Phys. Lett.* **104** 063903
[54] Ma J, Kuciauskas D, Albin D, Bhattacharya R, Reese M, Barnes T, Li J V, Gessert T and Wei S H 2013 Dependence of the minority-carrier lifetime on the stoichiometry of CdTe using time-resolved photoluminescence and first-principles calculations *Phys. Rev. Lett.* **111** 067402
[55] Yin W-J, Yang J-H, Kang J, Yan Y and Wei S-H 2015 Halide perovskite materials for solar cells: a theoretical review *J. Mater. Chem.* A **3** 8926–42
[56] Park J S, Kim S, Xie Z J and Walsh A 2018 Point defect engineering in thin-film solar cells *Nat. Rev. Mater.* **3** 194–210
[57] Kurchin R C, Gorai P, Buonassisi T and Stevanović V 2018 Structural and chemical features giving rise to defect tolerance of binary semiconductors *Chem. Mater.* **30** 5583–92
[58] Rai B P 1988 Cu_2O solar cells: a review *Sol. Cells* **25** 265–72
[59] Liu Y, Zhu J, Cai L, Yao Z, Duan C, Zhao Z, Zhao C and Mai W 2019 Solution-processed high-quality Cu_2O thin films as hole transport layers for pushing the conversion efficiency limit of Cu_2O/Si heterojunction solar cells *Solar RRL* **4** 1900339
[60] Minami T, Nishi Y and Miyata T 2016 Efficiency enhancement using a $Zn_{1-x}Ge_x$-O thin film as an n-type window layer in Cu_2O-based heterojunction solar cells *Appl. Phys. Express* **9** 052301
[61] Feldberg N, Keen B, Aldous J D, Scanlon D O, Stampe P A, Kennedy R J, Reeves R J, Veal T D and Durbin S M 2012 $ZnSnN_2$: a new earth-abundant element semiconductor for solar cells *2012 38th IEEE Photovoltaic Specialists Conf.* pp 002524–7
[62] Javaid K, Wu W, Wang J, Fang J, Zhang H, Gao J, Zhuge F, Liang L and Cao H 2018 Band offset engineering in $ZnSnN_2$-based heterojunction for low-cost solar cells *ACS Photonics* **5** 2094–9
[63] Wang W, Winkler M T, Gunawan O, Gokmen T, Todorov T K, Zhu Y and Mitzi D B 2014 Device characteristics of CZTSSe thin-film solar cells with 12.6% efficiency *Adv. Energy Mater.* **4** 1301465
[64] Noguchi H, Setiyadi A, Tanamura H, Nagatomo T and Omoto O 1994 Characterization of vacuum-evaporated tin sulfide film for solar cell materials *Sol. Energy Mater. Sol. Cells* **35** 325–31
[65] Banai R E, Horn M W and Brownson J R S 2016 A review of tin (II) monosulfide and its potential as a photovoltaic absorber *Sol. Energy Mater. Sol. Cells* **150** 112–29
[66] Sinsermsuksakul P, Sun L, Lee S W, Park H H, Kim S B, Yang C and Gordon R G 2014 Overcoming efficiency limitations of SnS-based solar cells *Adv. Energy Mater.* **4** 1400496
[67] Hall R B and Meakin J D 1979 The design and fabrication of high efficiency thin film CdS/Cu_2S solar cells *Thin Solid Films* **63** 203–11
[68] Xu Q, Huang B, Zhao Y, Yan Y, Noufi R and Wei S-H 2012 Crystal and electronic structures of Cu_xS solar cell absorbers *Appl. Phys. Lett.* **100** 061906
[69] Lukashev P, Lambrecht W R L, Kotani T and Van Schilfgaarde M 2007 Electronic and crystal structure of $Cu_{2-x}S$: full-potential electronic structure calculations *Phys. Rev.* B **76** 195202
[70] Barman S K and Huda M N 2020 First-principles study on the effect of Sn doping in Cu_2S—Acanthite phase as a substitute to low chalcocite for modeling complex doping *J. Appl. Phys.* **128** 015703
[71] Wong L H, Zakutayev A, Major J D, Hao X, Walsh A, Todorov T K and Saucedo E 2019 Emerging inorganic solar cell efficiency tables (Version 1) *J. Phys. Energy* **1** 032001
[72] Blank B, Kirchartz T, Lany S and Rau U 2017 Selection metric for photovoltaic materials screening based on detailed-balance analysis *Phys. Rev. Appl.* **8** 024032
[73] Yu L and Zunger A 2012 Identification of potential photovoltaic absorbers based on first-principles spectroscopic screening of materials *Phys. Rev. Lett.* **108** 068701
[74] Niemeyer M, Ohlmann J, Walker A W, Kleinschmidt P, Lang R, Hannappel T, Dimroth F and Lackner D 2017 Minority carrier diffusion length, lifetime and mobility in p-type GaAs and GaInAs *J. Appl. Phys.* **122** 115702
[75] Poindexter J R, Barnard E S, Kurchin R C and Buonassisi T 2018 Charge-carrier lifetime measurements in early-stage photovoltaic materials: intuition, uncertainties, and opportunities (arXiv:1805.05832)
[76] Maiberg M, Hölscher T, Jarzembowski E, Hartnauer S, Zahedi-Azad S, Fränzel W and Scheer R 2017 Verification of minority carrier traps in Cu(In,Ga)Se_2 and $Cu_2ZnSnSe_4$ by means of time-resolved photoluminescence *Thin Solid Films* **633** 208–12
[77] Hages C J, Redinger A, Levcenko S, Hempel H, Koeper M J, Agrawal R, Greiner D, Kaufmann C A and Unold T 2017 Identifying the real minority carrier lifetime in nonideal semiconductors: a case study of kesterite materials *Adv. Energy Mater.* **7** 1700167
[78] Arca E, Fioretti A, Lany S, Tamboli A C, Teeter G, Melamed C, Pan J, Wood K N, Toberer E and Zakutayev A 2018 Band edge positions and their impact on the simulated device performance of $ZnSnN_2$-based solar cells *IEEE J. Photovoltaics* **8** 110–7
[79] Xing G, Mathews N, Sun S, Lim S S, Lam Y M, Gratzel M, Mhaisalkar S and Sum T C 2013 Long-range balanced electron- and hole-transport lengths in organic-inorganic $CH_3NH_3PbI_3$ *Science* **342** 344–7
[80] Sze S M and Lee M-K 2012 *Semiconductor Devices: Physics and Technology* 3rd edn (New York: Wiley)
[81] Zunger A 2003 Practical doping principles *Appl. Phys. Lett.* **83** 57–59
[82] Wei S-H 2004 Overcoming the doping bottleneck in semiconductors *Comput. Mater. Sci.* **30** 337–48
[83] Robertson J and Clark S J 2011 Limits to doping in oxides *Phys. Rev.* B **83** 075205
[84] Whittles T J *et al* 2019 Band alignments, band gap, core levels, and valence band states in Cu_3BiS_3 for photovoltaics *ACS Appl. Mater. Interfaces* **11** 27033–47
[85] Whittles T J *et al* 2017 Core levels, band alignments, and valence-band states in $CuSbS_2$ for solar cell applications *ACS Appl. Mater. Interfaces* **9** 41916–26
[86] Rodríguez-Lazcano Y, Nair M T S and Nair P K 2001 $CuSbS_2$ thin film formed through annealing chemically deposited Sb_2S_3–CuS thin films *J. Cryst. Growth* **223** 399–406
[87] Ornelas-Acosta R E, Shaji S, Avellaneda D, Castillo G A, Das Roy T K and Krishnan B 2015 Thin films of copper antimony sulfide: a photovoltaic absorber material *Mater. Res. Bull.* **61** 215–25
[88] Paudel T R and Lambrecht W R L 2008 First-principles study of phonons and related ground-state properties and spectra in Zn-IV-N_2 compounds *Phys. Rev.* B **78** 115204
[89] Martinez A D, Fioretti A N, Toberer E S and Tamboli A C 2017 Synthesis, structure, and optoelectronic properties of II-IV-V_2 materials *J. Mater. Chem.* A **5** 11418–35

[90] Punya A and Lambrecht W R L 2013 Band offsets between $ZnGeN_2$, GaN, ZnO, and $ZnSnN_2$ and their potential impact for solar cells *Phys. Rev.* B **88** 075302
[91] Quayle P C, He K, Shan J and Kash K 2013 Synthesis, lattice structure, and band gap of $ZnSnN_2$ *MRS Commun.* **3** 135–8
[92] Sun S *et al* 2019 Accelerated development of perovskite-inspired materials via high-throughput synthesis and machine-learning diagnosis *Joule* **3** 1437–51
[93] Lee L C, Huq T N, MacManus-Driscoll J L and Hoye R L Z 2018 Research update: bismuth-based perovskite-inspired photovoltaic materials *APL Mater.* **6** 084502
[94] Ali R, Hou G-J, Zhu Z-G, Yan Q-B, Zheng Q-R and Su G 2018 Predicted lead-free perovskites for solar cells *Chem. Mater.* **30** 718–28
[95] Xu J *et al* 2020 Triple-halide wide–band gap perovskites with suppressed phase segregation for efficient tandems *Science* **367** 1097–104
[96] Hoye R L Z *et al* 2017 Strongly enhanced photovoltaic performance and defect physics of air-stable bismuth oxyiodide (BiOI) *Adv. Mater.* **29** 1702176
[97] Burton L A and Walsh A 2013 Band alignment in SnS thin-film solar cells: possible origin of the low conversion efficiency *Appl. Phys. Lett.* **102** 132111
[98] Whittles T J, Burton L A, Skelton J M, Walsh A, Veal T D and Dhanak V R 2016 Band alignments, valence bands, and core levels in the tin sulfides SnS, SnS_2, and Sn_2S_3: experiment and theory *Chem. Mater.* **28** 3718–26
[99] Shiel H *et al* 2020 Natural band alignments and band offsets of Sb_2Se_3 solar cells *ACS Appl. Mater.* **3** 11617–26
[100] Arca E *et al* 2019 Zn_2SbN_3: growth and characterization of a metastable photoactive semiconductor *Mater. Horiz.* **6** 1669–74
[101] Wei S-H and Zunger A 1998 Calculated natural band offsets of all II–VI and III–V semiconductors: chemical trends and the role of cation d orbitals *Appl. Phys. Lett.* **72** 2011–3
[102] Wang T, Ni C and Janotti A 2017 Band alignment and p-type doping of $ZnSnN_2$ *Phys. Rev.* B **95** 205205
[103] Butler K T, Frost J M and Walsh A 2015 Band alignment of the hybrid halide perovskites $CH_3NH_3PbCl_3$, $CH_3NH_3PbBr_3$ and $CH_3NH_3PbI_3$ *Mater. Horiz.* **2** 228–31
[104] Wallace S K, Butler K T, Hinuma Y and Walsh A 2019 Finding a junction partner for candidate solar cell absorbers enargite and bournonite from electronic band and lattice matching *J. Appl. Phys.* **125** 055703
[105] Anderson R L 1960 Germanium-gallium arsenide heterojunctions[Letter to the Editor] *IBM J. Res. Dev.* **4** 283–7
[106] Klein A 2012 Energy band alignment at interfaces of semiconducting oxides: a review of experimental determination using photoelectron spectroscopy and comparison with theoretical predictions by the electron affinity rule, charge neutrality levels, and the common anion rule *Thin Solid Films* **520** 3721–8
[107] Schlaf R, Lang O, Pettenkofer C and Jaegermann W 1999 Band lineup of layered semiconductor heterointerfaces prepared by van der Waals epitaxy: charge transfer correction term for the electron affinity rule *J. Appl. Phys.* **85** 2732–53
[108] Niles D W and Margaritondo G 1986 Heterojunctions: definite breakdown of the electron affinity rule *Phys. Rev.* B **34** 2923–5
[109] Tersoff J 1984 Schottky barrier heights and the continuum of gap states *Phys. Rev. Lett.* **52** 465–8
[110] Tejedor C and Flores F 1977 A simple approach to heterojunctions *J. Phys. C: Solid State Phys.* **11** L19–L23
[111] Heine V 1965 Theory of surface states *Phys. Rev.* **138** A1689–96
[112] Inkson J C 1980 Deep impurities in semiconductors. I. Evanescent states and complex band structure *J. Phys. C: Solid State Phys.* **13** 369–81
[113] Mönch W 2001 *Semiconductor Surfaces and Interfaces* (Berlin: Springer)
[114] Walukiewicz W 1989 Amphoteric native defects in semiconductors *Appl. Phys. Lett.* **54** 2094–6
[115] Walukiewicz W 1988 Mechanism of Fermi-level stabilization in semiconductors *Phys. Rev.* B **37** 4760–3
[116] Van De Walle C G and Neugebauer J 2003 Universal alignment of hydrogen levels in semiconductors, insulators and solutions *Nature* **423** 626–8
[117] Swallow J E N, Varley J B, Jones L A H, Gibbon J T, Piper L F J, Dhanak V R and Veal T D 2019 Transition from electron accumulation to depletion at β-Ga_2O_3 surfaces: the role of hydrogen and the charge neutrality level *APL Mater.* **7** 022528
[118] Kraut E A, Grant R W, Waldrop J R and Kowalczyk S P 1980 Precise determination of the valence-band edge in x-ray photoemission spectra—application to measurement of semiconductor interface potentials *Phys. Rev. Lett.* **44** 1620–3
[119] Kraut E A, Grant R W, Waldrop J R and Kowalczyk S P 1983 Semiconductor core-level to valence-band maximum binding-energy differences—precise determination by x-ray photoelectron-spectroscopy *Phys. Rev.* B **28** 1965–77
[120] Tanuma S, Powell C J and Penn D R 1994 Calculations of electron inelastic mean free paths. V. Data for 14 organic compounds over the 50–2000 eV range *Surf. Interface Anal.* **21** 165–76
[121] Powell C J and Jablonski A 2010 *NIST Electron Inelastic-Mean-Free-Path Database—Version 1.2* (Gaithersburg, MD: National Institute of Standards and Technology)
[122] Regoutz A, Mascheck M, Wiell T, Eriksson S K, Liljenberg C, Tetzner K, Williamson B A D, Scanlon D O and Palmgren P 2018 A novel laboratory-based hard X-ray photoelectron spectroscopy system *Rev. Sci. Instrum.* **89** 073105
[123] Siol S, Mann J, Newman J, Miyayama T, Watanabe K, Schmutz P, Cancellieri C and Jeurgens L P H 2020 Concepts for chemical state analysis at constant probing depth by lab-based XPS/HAXPES combining soft and hard X-ray sources *Surf. Interface Anal.* **52** 802–10
[124] Klein A 2015 Energy band alignment in chalcogenide thin film solar cells from photoelectron spectroscopy *J. Phys.: Condens. Matter* **27** 134201
[125] Siol S, Hellmann J C, Tilley S D, Graetzel M, Morasch J, Deuermeier J, Jaegermann W and Klein A 2016 Band alignment engineering at Cu_2O/ZnO heterointerfaces *ACS Appl. Mater. Interfaces* **8** 21824–31
[126] Deuermeier J, Gassmann J, Brötz J and Klein A 2011 Reactive magnetron sputtering of Cu_2O: dependence on oxygen pressure and interface formation with indium tin oxide *J. Appl. Phys.* **109** 113704
[127] Wilson S S, Bosco J P, Tolstova Y, Scanlon D O, Watson G W and Atwater H A 2014 Interface stoichiometry control to improve device voltage and modify band alignment in ZnO/Cu_2O heterojunction solar cells *Energy Environ. Sci.* **7** 3606–10
[128] Katsube R, Kazumi K, Tadokoro T and Nose Y 2018 Reactive epitaxial formation of a Mg–P–Zn ternary semiconductor in Mg/Zn_3P_2 solar cells *ACS Appl. Mater. Interfaces* **10** 36102–7
[129] Bosco J P, Scanlon D O, Watson G W, Lewis N S and Atwater H A 2013 Energy-band alignment of II–VI/Zn_3P_2 heterojunctions from x-ray photoemission spectroscopy *J. Appl. Phys.* **113** 203705
[130] Pan J, Cordell J, Tucker G J, Tamboli A C, Zakutayev A and Lany S 2019 Interplay between composition, electronic structure, disorder, and doping due to dual sublattice mixing in nonequilibrium synthesis of $ZnSnN_2$:O *Adv. Mater.* **31** 1807406

[131] Lany S, Fioretti A N, Zawadzki P P, Schelhas L T, Toberer E S, Zakutayev A and Tamboli A C 2017 Monte Carlo simulations of disorder in $ZnSnN_2$ and the effects on the electronic structure *Phys. Rev. Mater.* **1** 035401
[132] Hamilton D C, Arca E, Pan J, Siol S, Young M, Lany S and Zakutayev A 2019 Electron scattering mechanisms in polycrystalline sputtered zinc tin oxynitride thin films *J. Appl. Phys.* **126** 035701
[133] Javaid K, Yu J, Wu W, Wang J, Zhang H, Gao J, Zhuge F, Liang L and Cao H 2018 Thin film solar cell based on $ZnSnN_2$/SnO heterojunction *Phys. Status Solidi RRL* **12** 1700332
[134] Béchu S, Ralaiarisoa M, Etcheberry A and Schulz P 2020 Photoemission spectroscopy characterization of halide perovskites *Adv. Energy Mater.* **10** 1904007
[135] Broberg D, Medasani B, Zimmermann N E R, Yu G, Canning A, Haranczyk M, Asta M and Hautier G 2018 PyCDT: a Python toolkit for modeling point defects in semiconductors and insulators *Comput. Phys. Commun.* **226** 165–79
[136] Goyal A, Gorai P, Peng H, Lany S and Stevanović V 2017 A computational framework for automation of point defect calculations *Comput. Mater. Sci.* **130** 1–9
[137] Lany S and Zunger A 2008 Assessment of correction methods for the band-gap problem and for finite-size effects in supercell defect calculations: case studies for ZnO and GaAs *Phys. Rev.* B **78** 235104
[138] Kumagai Y and Oba F 2014 Electrostatics-based finite-size corrections for first-principles point defect calculations *Phys. Rev.* B **89** 195205
[139] De Wolf S, Holovsky J, Moon S-J, Löper P, Niesen B, Ledinsky M, Haug F-J, Yum J-H and Ballif C 2014 Organometallic halide perovskites: sharp optical absorption edge and its relation to photovoltaic performance *J. Phys. Chem. Lett.* **5** 1035–9
[140] Savory Christopher N and Scanlon D O 2019 The complex defect chemistry of antimony selenide *J. Mater. Chem.* A **7** 10739–44
[141] Azarhoosh P, McKechnie S, Frost J M, Walsh A and Van Schilfgaarde M 2016 Research Update: relativistic origin of slow electron-hole recombination in hybrid halide perovskite solar cells *APL Mater.* **4** 091501
[142] Kondrotas R, Chen C and Tang J 2018 Sb_2S_3 solar cells *Joule* **2** 857–78
[143] Tamilselvan M, Byregowda A, Su C-Y, Tseng C-J and Bhattacharyya A J 2019 Planar heterojunction solar cell employing a single-source precursor solution-processed Sb_2S_3 thin film as the light absorber *ACS Omega* **4** 11380–7
[144] Moon S-J, Itzhaik Y, Yum J-H, Zakeeruddin S M, Hodes G and Grätzel M 2010 Sb2S3-based mesoscopic solar cell using an organic hole conductor *J. Phys. Chem. Lett.* **1** 1524–7
[145] Deng H *et al* 2019 Quasiepitaxy strategy for efficient full-inorganic Sb2S3 solar cells *Adv. Funct. Mater.* **29** 1901720
[146] Choi Y C, Lee D U, Noh J H, Kim E K and Seok S I 2014 Highly improved Sb2S3 sensitized-inorganic–organic heterojunction solar cells and quantification of traps by deep-level transient spectroscopy *Adv. Funct. Mater.* **24** 3587–92
[147] Choi Y C, Hwang E and Kim D-H 2018 Controlled growth of SbSI thin films from amorphous Sb_2S_3 for low-temperature solution processed chalcohalide solar cells *APL Mater.* **6** 121108
[148] Nie R, Yun H-S, Paik M-J, Mehta A, Park B-W, Choi Y C and Seok S I 2018 Efficient solar cells based on light-harvesting antimony sulfoiodide *Adv. Energy Mater.* **8** 1701901
[149] Ma S, Yang Y, Liu C, Cai M, Ding Y, Tan Z A, Shi P, Dai S, Alsaedi A and Hayat T 2019 Vertically oriented BiI_3 template featured BiI_3/polymer heterojunction for high photocurrent and long-term stable solar cells *ACS Appl. Mater. Interfaces* **11** 32509–16
[150] Hamdeh U H, Nelson R D, Ryan B J, Bhattacharjee U, Petrich J W and Panthani M G 2016 Solution-processed BiI_3 thin films for photovoltaic applications: improved carrier collection via solvent annealing *Chem. Mater.* **28** 6567–74
[151] Tiwari D, Alibhai D and Fermin D J 2018 Above 600 mV open-circuit voltage BiI_3 solar cells *ACS Energy Lett.* **3** 1882–6
[152] Brandt R E *et al* 2015 Investigation of bismuth triiodide (BiI_3) for photovoltaic applications *J. Phys. Chem. Lett.* **6** 4297–302
[153] Ganose A M, Butler K T, Walsh A and Scanlon D O 2016 Relativistic electronic structure and band alignment of BiSI and BiSeI: candidate photovoltaic materials *J. Mater. Chem.* A **4** 2060–8
[154] Hahn N T, Self J L and Mullins C B 2012 BiSI micro-rod thin films: efficient solar absorber Electrodes? *J. Phys. Chem. Lett.* **3** 1571–6
[155] Huq T N *et al* 2020 Electronic structure and optoelectronic properties of bismuth oxyiodide robust against percent-level iodine-, oxygen-, and bismuth-related surface defects *Adv. Funct. Mater.* **30** 1909983
[156] Li Z *et al* 2019 9.2%-efficient core-shell structured antimony selenide nanorod array solar cells *Nat. Commun.* **10** 125
[157] Major J 2020 Step up in performance *Nat. Energy* **5** 559–60
[158] Tang R *et al* 2020 Hydrothermal deposition of antimony selenosulfide thin films enables solar cells with 10% efficiency *Nat. Energy* **5** 587–95
[159] Yang Z *et al* 2019 Ultrafast self-trapping of photoexcited carriers sets the upper limit on antimony trisulfide photovoltaic devices *Nat. Commun.* **10** 4540
[160] Ganose A M, Matsumoto S, Buckeridge J and Scanlon D O 2018 Defect engineering of earth-abundant solar absorbers BiSI and BiSeI *Chem. Mater.* **30** 3827–35
[161] Maughan A E, Ganose A M, Bordelon M M, Miller E M, Scanlon D O and Neilson J R 2016 Defect tolerance to intolerance in the vacancy-ordered double perovskite semiconductors Cs_2SnI_6 and Cs_2TeI_6 *J. Am. Chem. Soc.* **138** 8453–64
[162] Yin Y, Huang Y, Wu Y, Chen G, Yin W-J, Wei S-H and Gong X 2017 Exploring emerging photovoltaic materials beyond perovskite: the case of skutterudite *Chem. Mater.* **29** 9429–35
[163] Endres J *et al* 2016 Valence and conduction band densities of states of metal halide perovskites: a combined experimental–theoretical study *J. Phys. Chem. Lett.* **7** 2722–9
[164] Travis W, Glover E N K, Bronstein H, Scanlon D O and Palgrave R G 2016 On the application of the tolerance factor to inorganic and hybrid halide perovskites: a revised system *Chem. Sci.* **7** 4548–56
[165] Xu Q, Yang D, Lv J, Sun -Y-Y and Zhang L 2018 Perovskite solar absorbers: materials by design *Small Methods* **2** 1700316
[166] Sangalli D *et al* 2019 Many-body perturbation theory calculations using the yambo code *J. Phys.: Condens. Matter* **31** 325902
[167] Van Schilfgaarde M, Kotani T and Faleev S 2006 Quasiparticle self-consistent GW theory *Phys. Rev. Lett.* **96** 226402
[168] Brivio F, Butler K T, Walsh A and Van Schilfgaarde M 2014 Relativistic quasiparticle self-consistent electronic structure of hybrid halide perovskite photovoltaic absorbers *Phys. Rev.* B **89** 155204
[169] Golze D, Dvorak M and Rinke P 2019 The GW compendium: a practical guide to theoretical photoemission spectroscopy *Frontiers Chem.* **7** 377
[170] Kresse G and Furthmüller J 1996 Efficiency of *ab-initio* total energy calculations for metals and semiconductors using a plane-wave basis set *Comput. Mater. Sci.* **6** 15–50
[171] Kresse G and Furthmüller J 1996 Efficient iterative schemes for *ab initio* total-energy calculations using a plane-wave basis set *Phys. Rev.* B **54** 11169–86

[172] Clark S J, Segall M D, Pickard C J, Hasnip P J, Probert M I J, Refson K and Payne M C 2005 First principles methods using CASTEP *Z. Kristallogr.* **220** 567–70
[173] Blum V, Gehrke R, Hanke F, Havu P, Havu V, Ren X, Reuter K and Scheffler M 2009 *Ab initio* molecular simulations with numeric atom-centered orbitals *Comput. Phys. Commun.* **180** 2175–96
[174] Giannozzi P *et al* 2009 QUANTUM ESPRESSO: a modular and open-source software project for quantum simulations of materials *J. Phys.: Condens. Matter* **21** 395502
[175] Mortensen J J, Hansen L B and Jacobsen K W 2005 Real-space grid implementation of the projector augmented wave method *Phys. Rev.* B **71** 035109
[176] Martin R M 2004 *Electronic Structure: Basic Theory and Practical Methods* (Cambridge: Cambridge University Press)
[177] Giustino F 2014 *Materials Modelling Using Density Functional Theory. Properties and Predictions* (Oxford: Oxford University Press (OUP))
[178] Jackson A J, Ganose A M, Regoutz A, Egdell R G and Scanlon D O 2018 Galore: broadening and weighting for simulation of photoelectron spectroscopy *J. Open Source Softw.* **3** 773
[179] Vasheghani Farahani S K, Veal T D, Mudd J J, Scanlon D O, Watson G W, Bierwagen O, White M E, Speck J S and McConville C F 2014 Valence-band density of states and surface electron accumulation in epitaxial SnO_2 films *Phys. Rev.* B **90** 155413
[180] Birkett M *et al* 2018 Band gap temperature-dependence and exciton-like state in copper antimony sulphide, $CuSbS_2$ *APL Mater.* **6** 084904
[181] Sholl D S and Steckel J A 2009 *Density Functional Theory: A Practical Introduction* (New York: Wiley)
[182] Walsh A and Butler K T 2014 Prediction of electron energies in metal oxides *Acc. Chem. Res.* **47** 364–72
[183] Butler K T, Hendon C H and Walsh A 2014 Electronic chemical potentials of porous metal–organic frameworks *J. Am. Chem. Soc.* **136** 2703–6
[184] Sinsermsuksakul P, Hartman K, Bok Kim S, Heo J, Sun L, Hejin Park H, Chakraborty R, Buonassisi T and Gordon R G 2013 Enhancing the efficiency of SnS solar cells via band-offset engineering with a zinc oxysulfide buffer layer *Appl. Phys. Lett.* **102** 053901
[185] Tiwari D, Cardoso-Delgado F, Alibhai D, Mombrú M and Fermín D J 2019 Photovoltaic performance of phase-pure orthorhombic BiSI thin-films *ACS Appl. Mater.* **2** 3878–85
[186] Butler K T, Kumagai Y, Oba F and Walsh A 2016 Screening procedure for structurally and electronically matched contact layers for high-performance solar cells: hybrid perovskites *J. Mater. Chem.* C **4** 1149–58
[187] Butler K T (available at: https://github.com/keeeto/ElectronicLatticeMatch)
[188] Li Y-H, Walsh A, Chen S, Yin W-J, Yang J-H, Li J, Silva J L F D, Gong X G and Wei S-H 2009 Revised *ab initio* natural band offsets of all group IV, II–VI, and III–V semiconductors *Appl. Phys. Lett.* **94** 212109
[189] Patrick C E and Giustino F 2011 Structural and electronic properties of semiconductor-sensitized solar-cell interfaces *Adv. Funct. Mater.* **21** 4663–7
[190] Zhu B, Schusteritsch G, Lu P, MacManus-Driscoll J L and Pickard C J 2019 Determining interface structures in vertically aligned nanocomposite films *APL Mater.* **7** 061105
[191] Favaro M, Jeong B, Ross P N, Yano J, Hussain Z, Liu Z and Crumlin E J 2016 Unravelling the electrochemical double layer by direct probing of the solid/liquid interface *Nat. Commun.* **7** 12695
[192] Axnanda S *et al* 2015 Using 'tender' x-ray ambient pressure x-ray photoelectron spectroscopy as a direct probe of solid-liquid interface *Sci. Rep.* **5** 9788
[193] Stoerzinger K A, Hong W T, Crumlin E J, Bluhm H and Shao-Horn Y 2015 Insights into electrochemical reactions from ambient pressure photoelectron spectroscopy *Acc. Chem. Res.* **48** 2976–83
[194] Schnadt J, Knudsen J and Johansson N 2020 Present and new frontiers in materials research by ambient pressure x-ray photoelectron spectroscopy *J. Phys.: Condens. Matter* **32** 413003
[195] Arble C, Jia M and Newberg J T 2018 Lab-based ambient pressure X-ray photoelectron spectroscopy from past to present *Surf. Sci. Rep.* **73** 37–57
[196] Lichterman M F *et al* 2015 Direct observation of the energetics at a semiconductor/liquid junction by operando X-ray photoelectron spectroscopy *Energy Environ. Sci.* **8** 2409–16
[197] Stoerzinger K A, Du Y, Spurgeon S R, Wang L, Kepaptsoglou D, Ramasse Q M, Crumlin E J and Chambers S A 2018 Chemical and electronic structure analysis of a $SrTiO_3$ (001)/p-Ge (001) hydrogen evolution photocathode *MRS Commun.* **8** 446–52
[198] Shavorskiy A *et al* 2017 Direct mapping of band positions in doped and undoped hematite during photoelectrochemical water splitting *J. Phys. Chem. Lett.* **8** 5579–86
[199] Vanka S, Arca E, Cheng S, Sun K, Botton G A, Teeter G and Mi Z 2018 High efficiency Si photocathode protected by multifunctional GaN nanostructures *Nano Lett.* **18** 6530–7
[200] Tilley S D 2019 Recent advances and emerging trends in photo-electrochemical solar energy conversion *Adv. Energy Mater.* **9** 1802877
[201] Zhang X, Yang H, Zhang B, Shen Y and Wang M 2016 BiOI–TiO_2 nanocomposites for photoelectrochemical water splitting *Adv. Mater. Interface* **3** 1500273